

DENSE GAS IN MOLECULAR CORES ASSOCIATED WITH *PLANCK* GALACTIC COLD CLUMPS

JINGHUA YUAN (袁敬华)¹, YUEFANG WU^{2†}, TIE LIU³, TIANWEI ZHANG⁴, JIN ZENG LI¹, HONG-LI LIU¹, FANYI MENG⁵, PING CHEN², RUNJIE HU², AND KE WANG⁶

¹National Astronomical Observatories, Chinese Academy of Sciences, 20A Datun Road, Chaoyang District, Beijing 100012, China;

²Department of Astronomy, Peking University, 100871 Beijing, China;

³Korea Astronomy and Space Science Institute 776, Daedeokdae-ro, Yuseong-gu, Daejeon, Republic of Korea 305-348;

⁴Peking University Health Science Center, Xueyuan Road 38th, Haidian District, Beijing 100191, China;

⁵Physikalisches Institut, Universitat zu Koln, Zulpicher Str. 77, 50937, Germany; and

⁶European Southern Observatory, Karl-Schwarzschild-Str. 2, D-85748 Garching bei Munchen, Germany

Draft Version, June 30, 2021

ABSTRACT

We present the first survey of dense gas towards *Planck* Galactic Cold Clumps (PGCCs). Observations in the $J = 1 - 0$ transitions of HCO^+ and HCN towards 621 molecular cores associated with PGCCs were performed using the Purple Mountain Observatory 13.7-m telescope. Among them, 250 sources have detection, including 230 cores detected in HCO^+ and 158 in HCN . Spectra of the $J = 1 - 0$ transitions from ^{12}CO , ^{13}CO , and C^{18}O at the centers of the 250 cores were extracted from previous mapping observations to construct a multi-line data set. The significantly low detection rate of asymmetric double-peaked profiles, together with the well consistence among central velocities of CO , HCO^+ , and HCN spectra, suggests that the CO-selected *Planck* cores are more quiescent compared to classical star-forming regions. The small difference between line widths of C^{18}O and HCN indicates that the inner regions of CO-selected *Planck* cores are not more turbulent than the exterior. The velocity-integrated intensities and abundances of HCO^+ are positively correlated with those of HCN , suggesting these two species are well coupled and chemically connected. The detected abundances of both HCO^+ and HCN are significantly lower than values in other low- to high-mass star-forming regions. The low abundances may be due to beam dilution. On the basis of the inspection of the parameters given in the PGCC catalog, we suggest that there may be about 1 000 PGCC objects having sufficient reservoir of dense gas to form stars.

Keywords: ISM: abundances – ISM: clouds – ISM: kinematics and dynamics – ISM: molecular – stars: formation

1. INTRODUCTION

Stars form in dense regions of molecular clouds. However, some physical and chemical properties of cold compact objects that breed stars are still poorly understood. A key approach would be to statistically investigate cold dense clumps in the Galaxy. In the last decade, numerous dense clumps revealed by surveys in continuum at (sub-)millimeter domain using ground-based facilities and the *Herschel Space Observatory* (e.g. Schuller et al. 2009; Andre et al. 2010; Molinari et al. 2010; Aguirre et al. 2011) have led to significant advancement. However, these surveys are mainly confined in the Galactic plane and several well-known nearby star-forming regions, an all-sky survey at multi-bands is crucial to the understanding of star formation in different environments.

The *Planck* satellite (Tauber et al. 2010; Planck Collaboration et al. 2011a) carried out the first all-sky survey at multi-bands in the submm-to-mm range with unprecedented sensitivity and provides an inventory of cold condensations of interstellar matter in the Galaxy. The first all-sky Cold Clump Catalogue of *Planck* Objects (C3PO) released in Planck Collaboration et al. (2011d) consists of 10,342 cold sources that stand out against a warmer environment. The C3PO clumps are cold with dust temperatures ranging from 7 K to 19 K, with a distribution peaking around 13 K. A detailed analysis of ten C3PO clumps carried out by Planck Collaboration et al. (2011c) revealed low column densities of N_{H_2} $(0.1 - 1.6) \times 10^{22} \text{ cm}^{-2}$ which can only be treated as lower

limits due to the poor resolution of *Planck* bands. Among the C3PO clumps, 915 early cold cores (ECCs) were identified based on criteria of $S/N > 15$ and $T < 14 \text{ K}$ where S/N is the signal-to-noise ratio. The ECC sample is delivered as a part of the *Planck* Early Release Compact Source Catalogue (ERCSC, Planck Collaboration et al. 2011b). As the high-S/N and cold tail of the C3PO objects, ECCs are excellent targets for studying the earliest stages of star formation (Juvela et al. 2010, 2011, 2012, 2015; Parikka et al. 2015). Recently, Planck Collaboration et al. (2015) released the *Planck* Catalog of Galactic Cold Clumps (PGCCs). As the full version of the ECC catalog, the PGCC catalog provides 13 188 Galactic sources spreading across the whole sky. Containing sources in very different environments, the PGCC catalog is useful for investigating the evolution from molecular clouds to cores.

To reveal the molecular characteristics, we carried out survey observations in the $J = 1 - 0$ transitions of ^{12}CO , ^{13}CO , and C^{18}O towards more than 600 *Planck* cold clumps selected from the ECC catalog in both single-pointing and on-the-fly modes (Wu et al. 2012; Liu et al. 2012, 2013a, 2015; Meng et al. 2013). We found that *Planck* cold clumps have the smallest line widths compared to other star-forming samples (e.g., IRDCs, Wang et al. 2009, 2014) indicating quiescent features and nature of very early evolutionary stages.

Although some kinematic properties have been revealed, the low critical densities of CO and its isotopologues prevent us investigating the denser inner regions. Observations in dense gas tracers are crucial to unveiling the physical and chemical features of the interior of these objects.

[†] ywu@pku.edu.cn

In this paper, we report on a survey of the $J = 1 - 0$ transitions of HCO^+ and HCN towards the smaller sub-structures enclosed in the ECCs which have been previously mapped in CO (see section 2). Combining spectra of CO and its isotopologues extracted from previous mapping observations, we have carried out a comprehensive study of dense gas in these sources. This paper is arranged as follows. We present a description of the sample and observations in Section 2 and the results in Section 3. In Section 4, we try to comprehensively discuss the data. The main findings are summarized in Section 5.

2. THE SAMPLE AND OBSERVATIONS

As mentioned in section 1, more than 600 *Planck* cold clumps have been mapped in the $J = 1 - 0$ transitions of ^{12}CO , ^{13}CO , and C^{18}O . A $22' \times 22'$ region for each clump was mapped with a spatial resolution of about $52''$. Only the central $14' \times 14'$ portion, where the sensitivity is high enough, have been taken into account. Details about the mapping observations are referred to Liu et al. (2012) and Meng et al. (2013). As demonstrated in Meng et al. (2013), we have identified sub-structures in regions defined by a contour of 60% of the peak intensity of ^{13}CO . In total, 621 smaller substructures have been identified (Liu et al. 2012; Meng et al. 2013, T. Zhang et al. in prep; P. Chen et al. in prep; R. Hu et al. in prep), and are referred as CO-selected cores in this work to be distinguished from the parental clumps. These CO-selected cores have source-averaged column densities ranging from $7.6 \times 10^{20} \text{ cm}^{-2}$ to $3.7 \times 10^{22} \text{ cm}^{-2}$ with a mean value of $7.2 \times 10^{21} \text{ cm}^{-2}$. The source-averaged volume densities are in the range of $(0.1 - 68.6) \times 10^3 \text{ cm}^{-3}$ with a mean of $4.6 \times 10^3 \text{ cm}^{-3}$. The low mean excitation temperature of CO ($\sim 11 \text{ K}$) suggests quiescent features. The distances to 164 CO-selected cores have been adopted from the PGCC catalog (Planck Collaboration et al. 2015). The distances to other 382 sources, whose distances are not provided in the PGCC catalog, are from Wu et al. (2012). Note that we have confined the Galactocentric distance to be smaller than 20 kpc while matching the sample with the catalogs of Wu et al. (2012) and Planck Collaboration et al. (2015). The distances range from 0.1 to 14.7 kpc with a mean value of 1.3 kpc.

Single-pointing observations of the CO-selected cores in $\text{HCO}^+ J = 1 - 0$ (89.189 GHz) and HCN $J = 1 - 0$ (88.632 GHz) were carried out using the Purple Mountain Observatory (PMO) 13.7-m telescope with the position-switch mode from June to July of 2013 and from May to June of 2014. The half power beam width (HPBW) and main beam efficiency at 89 GHz are about $59''$ and 55%, respectively. The pointing and tracking accuracies were both better than $5''$ determined by scanning solar planets. A double sideband SIS receiver was used to cover both lines in the upper sideband (USB) which has a width of 1 GHz allocated to 16384 channels (Shan et al. 2012). The spectral resolution is about 61 kHz, corresponding to a velocity resolution of 0.21 km s^{-1} . In our observations, the off position for each source was originally set to be $30'$ west away from the target along the right ascension direction. We have carefully checked the the off positions with direct observations to find that most of them are emission-free in both HCO^+ and HCN. For the five sources, which show anomalous absorption features in the spectra indicating possible line contamination, the off positions were reset to the opposite direction, i.e. $30'$ east from the target. The on-source time was about 5 minutes for most sources, and longer than 10 minutes for a small number of objects ob-

served in 2013. The system temperatures are in the range of 133 to 363 K, with a mean value of 190 K. The CLASS software of the GILDAS package (Pety 2005) was used to reduce the data. In order to achieve a higher sensitivity, we smoothed the spectra to a lower velocity resolution of 0.42 km s^{-1} . The final reduced spectra have 1σ noises ranging from 0.02 to 0.23 K, with a mean value of 0.07 K and a median of 0.06 K.

3. RESULTS

Among the 621 observed molecular cores, 250 ones have valid detection in either $\text{HCO}^+ J = 1 - 0$ or HCN $J = 1 - 0$, including 138 cores detected in both lines, 92 cores only detected in $\text{HCO}^+ J = 1 - 0$, and 20 cores only detected in HCN $J = 1 - 0$. The designations and coordinates of these 250 sources are given in the first three columns of Table 1. In Figure 1, they are represented with filled circles. We note that the spatial distribution of CO-selected cores is biased towards nearby star-forming regions (e.g., Perseus, Taurus and Orion) while the Galactic plane is under-represented. This is because of the higher confusion in the Galactic plane, so that the S/N tends to be lower there, but also because the dust temperatures in the plane tend to be higher conflicting to the selection criteria of ECCs (Planck Collaboration et al. 2011d). The distribution of the targets in the face-on Milky Way is shown in Figure 2. Most sources ($\sim 85\%$) reside in the 10 kpc inner region from the Galactic center with a concentration near the Sun. Example spectra of several sources are presented in Figure 3. Most sources have one velocity component except for four ones which show two velocity components. In all the 250 sources, 254 velocity components have been detected.

3.1. Observed Parameters

From previous mapping observations, we have extracted spectra of the $J = 1 - 0$ transitions of ^{12}CO , ^{13}CO and C^{18}O at the peak of each core to construct a data set with five lines. For spectra of ^{12}CO , ^{13}CO , C^{18}O and HCO^+ , peak intensities, centroid velocities, and line widths of all the 250 cores have been obtained by fitting Gaussian profiles.

For HCN $J = 1 - 0$, we have performed hyperfine structure fitting by initiating the intensity ratios of $I_{F=1-1}/I_{F=2-1} = 0.6$ and $I_{F=0-1}/I_{F=2-1} = 0.2$ using the HFS method in CLASS which resulted in four parameters $p1$, $p2$, $p3$, and $p4$. Here, $p2$ and $p3$ are the centroid velocity and line width. The intensities and optical depths of the main and satellite components can be expressed as functions of $p1$ and $p4$,

$$\begin{aligned} T_{\text{main}} &= \frac{p1}{p4} (1 - e^{-p4}), \\ T_{\text{satellite}} &= \frac{p1}{p4} (1 - e^{-R \cdot p4}), \\ \tau_{\text{main}} &= p4, \\ \tau_{\text{satellite}} &= R \cdot p4. \end{aligned} \quad (1)$$

Here, R is the intrinsic intensity ratio of the satellite component to the main component. The detailed procedure of the hyperfine fitting is referred to the online documents of the CLASS software¹. The resulting observational parameters for $\text{HCO}^+ J = 1 - 0$ and HCN $J = 1 - 0$ are given in Table 1.

3.2. Derived Parameters

¹ <http://www.iram.fr/IRAMFR/GILDAS/doc/html/class-html>

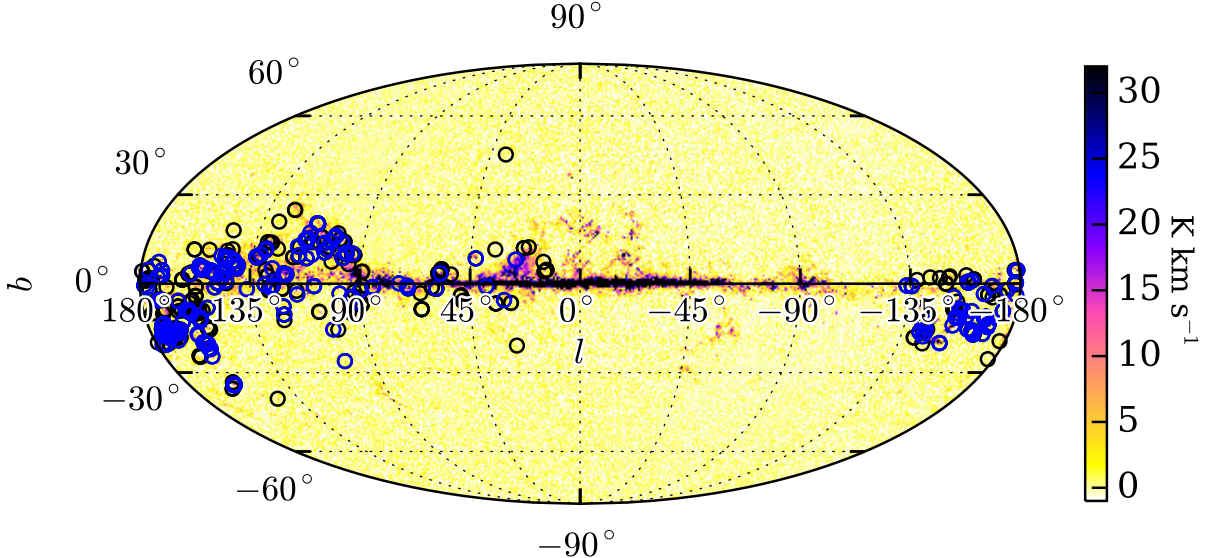


Figure 1. Spatial distribution of the observed sources (black circles) and the ones with valid detection (blue circles). The background shows CO $J = 1 - 0$ emission of the Type 3 map from Planck Collaboration et al. (2014).

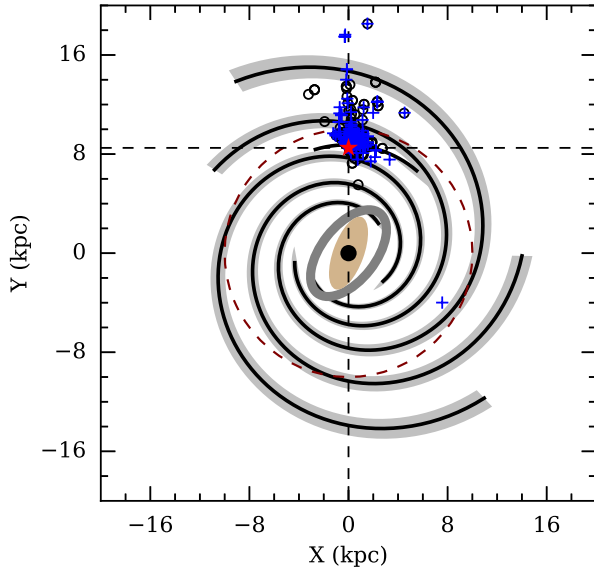


Figure 2. Spatial distribution of the sources with (blue crosses) and without (black circles) detection in the face-on Milky Way. The spiral arms are reproduced using the 4-arm model of Hou & Han (2014) with $R_0 = 8.5$ kpc and $\Theta_0 = 220 \text{ km s}^{-1}$ fitted to H II regions. The large dashed circle has a radius of 10 kpc.

For the sake of revealing physical features of these molecular cores, some fundamental parameters have been deduced from the observed spectra under the assumption of local thermal equilibrium (LTE). The measured brightness temperature (T_r) for a specific transition as a function of excitation temperature (T_{ex}) can be expressed as

$$T_r = \frac{h\nu}{k} [J(T_{\text{ex}}) - J(T_{\text{bg}})] \times [1 - \exp(-\tau)] f, \quad (2)$$

where $J(T) = [\exp(h\nu/kT) - 1]^{-1}$, $T_{\text{bg}} = 2.73$ K is the temperature of the cosmic background radiation, and f is the beam-filling factor. Under LTE condition, the optical depths of ^{12}CO and ^{13}CO can be straightforwardly obtained from comparing

the measured brightness temperatures:

$$\frac{T_r(^{12}\text{CO})}{T_r(^{13}\text{CO})} \approx \frac{1 - \exp(-\tau_{12})}{1 - \exp(-\tau_{13})}. \quad (3)$$

Here, $\tau_{12}/\tau_{13} = [^{12}\text{CO}]/[^{13}\text{CO}]$. The isotope ratio of $^{12}\text{C}/^{13}\text{C}$ for each source has been deduced from the following equation (Pineda et al. 2013),

$$\frac{^{12}\text{C}}{^{13}\text{C}} = 4.7 \frac{R_{\text{gal}}}{\text{kpc}} + 25.05, \quad (4)$$

where R_{gal} is the Galactocentric distance in kpc. With the derived optical depth, the excitation temperature can be reached from Equation 2 based on the intensity of ^{12}CO .

Under LTE condition, the column density of a linear molecule can be expressed as

$$N = \frac{3k}{8\pi^3 \nu \mu^2 S} \frac{Q_{\text{rot}}}{g_{J+1}} \frac{\exp\left(\frac{E_{\text{up}}}{kT_{\text{ex}}}\right)}{J(T_{\text{ex}})} \times \frac{1}{J(T_{\text{ex}}) - J(T_{\text{bg}})} \frac{\tau}{1 - \exp(-\tau)} \int T_r dv. \quad (5)$$

Here, μ is the permanent dipole moment of the molecule. For the $1 - 0$ transition, the line strength $S = \frac{J+1}{2J+3} = \frac{1}{3}$, the degeneracy $g_{J+1} = 2J + 3 = 3$, where J is the rotational quantum number of the lower state. We have followed McDowell (1988) to write the partition function as $Q_{\text{rot}} = \frac{kT}{hB} + \frac{1}{3}$ where B is the rotational constant. The molecular parameters have been adopted from the Cologne Database for Molecular Spectroscopy (CDMS)².

In the calculation, the excitation temperatures of ^{13}CO and C^{18}O have been assigned to be equal to that of ^{12}CO . This would be reasonable while considering the fact that ^{12}CO , ^{13}CO and C^{18}O are well coupled in ECCs (Wu et al. 2012). The optical depths and column densities of ^{13}CO have been obtained from Equations 3 and 5. For C^{18}O , we derived optical depths and column densities from Equations 2 and 5.

² <http://www.astro.uni-koeln.de/cdms/>

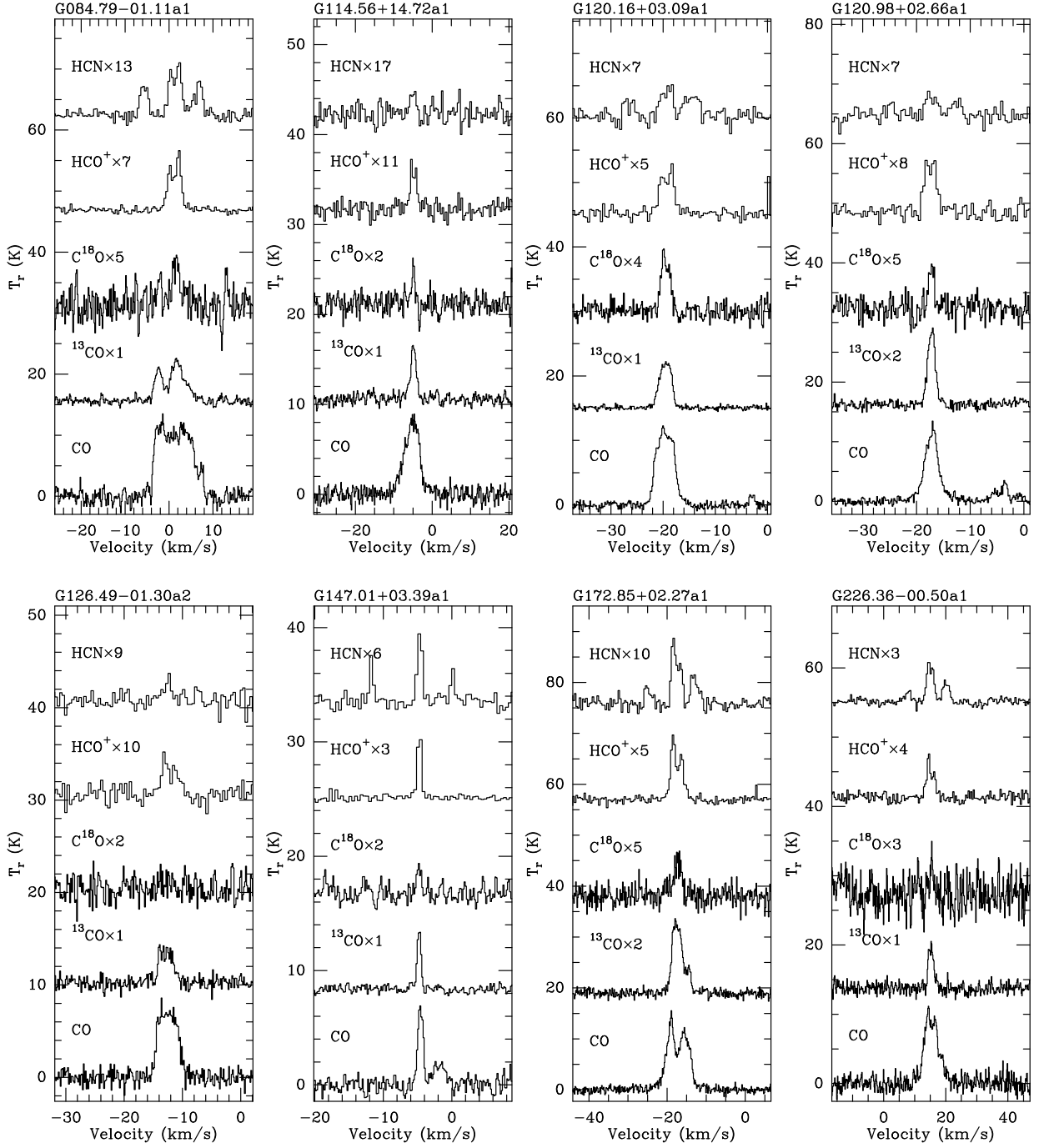


Figure 3. Example spectra.

For lacking observations of transitions from an isotopologue and a higher excitation level, the excitation temperatures of HCO^+ cannot be reliably derived. Additionally, optically thin feature for most sources (see Table 2) further prevented us obtaining estimates using Equation 2 under an optically thick assumption. In this work, we assumed the excitation temperatures of $\text{HCO}^+ J = 1 - 0$ to be its upper energy in Kelvin ($E_u/k = 4.28 \text{ K}$). Then the optical depths and column densities were derived from Equations 2 and 5. We note that the column densities obtained here are lower limits (e.g., Hatchell et al. 1998; Miettinen 2012, 2014) due to the use of upper energy as the excitation temperatures.

For HCN, the excitation temperatures were straightfor-

wardly derived from Equation 2 using optical depths obtained from HFS fitting (see section 3.1 and Table 1). For the derivation of column densities of HCN, Equation 5 was used by multiplying a factor of 1.8 which comes from the intensity ratios among the main and satellite components.

The column densities of CO for the 189 cores with detection in C^{18}O were calculated from that of C^{18}O with a consideration of isotope ratio of $^{16}\text{O}/^{18}\text{O}$ as a function of Galactocentric distance (Wilson & Rood 1994),

$$\frac{^{16}\text{O}}{^{18}\text{O}} = 58.8 \frac{R_{\text{gal}}}{\text{kpc}} + 37.1. \quad (6)$$

For sources without detection in $\text{C}^{18}\text{O} J = 1 - 0$, the CO col-

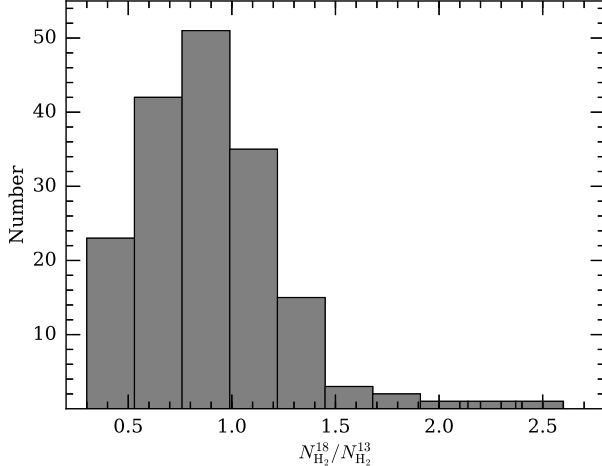


Figure 4. Distribution of the $N_{\text{H}_2}^{18}/N_{\text{H}_2}^{13}$ ratios for the 189 sources with C^{18}O detection.

umn densities were obtained from that of ^{13}CO by adopting isotope ratio given in Equation 4. Then the H_2 column densities were derived with the consideration of CO abundances as a function of Galactocentric distances (Fontani et al. 2012),

$$X_{\text{CO}} = 8.5 \times 10^{-5} \exp\left(1.105 - 0.13 \frac{R_{\text{gal}}}{\text{kpc}}\right). \quad (7)$$

In order to test the consistency between the two methods, we have obtained two sets of H_2 column densities of the 189 sources from C^{18}O and ^{13}CO and denoted them as $N_{\text{H}_2}^{18}$ and $N_{\text{H}_2}^{13}$. As shown in Figure 4, the $N_{\text{H}_2}^{18}/N_{\text{H}_2}^{13}$ ratios are ranging from 0.3 to 2.6 with a mean of 0.9 and a standard derivation of 0.3, indicating that the H_2 column densities derived from ^{13}CO and C^{18}O are consistent to each other.

One should note that the derived H_2 column densities would suffer from large uncertainties due to the abundance variations of CO. As noted in the literature the Galactic gradients of abundances (Equations 4, 6, and 7) would be valid in the Galactocentric distances between 3 kpc and 10 kpc where CO has significant emission (Wilson & Rood 1994; Pineda et al. 2013). As shown in Figure 2, most sources reside inside 10 kpc from the Galactic center. For these targets inside the 10 kpc circle, abundance ratios of $[^{12}\text{C}]/[^{13}\text{C}]$, $[^{16}\text{O}]/[^{18}\text{O}]$ and $[\text{CO}]/[\text{H}_2]$ have been obtained from Equations 4, 6, and 7. The $[^{12}\text{C}]/[^{13}\text{C}]$ ranges from 39 to 72, $[^{16}\text{O}]/[^{18}\text{O}]$ from 213 to 625, and $[\text{CO}]/[\text{H}_2]$ from 0.7×10^{-4} to 1.7×10^{-4} . For sources with Galactocentric distances larger than 10 kpc, the abundance ratios at $R_{\text{gal}} = 10$ kpc have been adopted. We compared the $[^{12}\text{C}]/[^{13}\text{C}]$ obtained from Equation 4 ratios to that from Wilson & Rood (1994) and found that the differences are smaller than 25%. We estimate that the variations of abundance ratios would introduce uncertainties smaller than a factor of one for sources with $R_{\text{gal}} < 10$ kpc. The uncertainties for sources with $R_{\text{gal}} > 10$ kpc would be larger.

The resulting optical depths of ^{13}CO , C^{18}O and HCO^+ , excitation temperatures of CO, column densities of ^{13}CO , C^{18}O , HCO^+ , and HCN are given in columns 4–11 of Table 2. The statistics of some derived parameters are presented in Table 3. The excitation temperatures in the CO-selected cores with HCO^+ and/or HCN detection range from 7.6 to 34.4 K, significantly higher than the values in Wu et al. (2012) and the dust temperatures (7–19 K, Planck Collaboration et al. 2011d).

The differences may be due to the sources in this work are relatively dense regions in clumps studied by Planck Collaboration et al. (2011d) and Wu et al. (2012). The mean excitation temperature is about 12.54 K approximately equal to the mean dust temperature (13 K, Planck Collaboration et al. 2011d) and slightly higher than the value in Wu et al. (2012). The excitation temperatures of these source with HCO^+ and/or HCN detection are significantly higher than that of CO-selected cores in the Taurus, Perseus, and California complexes (Meng et al. 2013), but similar to that of CO-selected cores in the Orion complex (Liu et al. 2012). The column densities of H_2 cover the range of $(1.5 - 70.9) \times 10^{21} \text{ cm}^{-2}$ with a mean value of $1.3 \times 10^{22} \text{ cm}^{-2}$, much higher than those of CO-selected cores in the Orion, Taurus, Perseus, and California complexes (Liu et al. 2012; Meng et al. 2013). This is a natural result because the sources with detection in HCO^+ and/or HCN are relative denser ones.

4. DISCUSSIONS

In order to assure the detection of HCO^+ and/or HCN is not purely distance and sensitivity limited, we have plotted histograms of distances and RMS noises of HCO^+ for CO-selected cores with and without detection. As shown in Figure 5(a), the distances for sources with and without detection have a similar distribution. The sources with detection in dense gas tracers have distances ranging from 0.1 to 14.7 kpc with a mean of 1.4 kpc and a median of 0.8 kpc. For sources without detection, the values range from 0.1 to 10.2 kpc with a mean of 1.2 kpc and a median value of 0.9 kpc. The similar mean and median values for source with and without detection suggest that distances have not induced biases to the detection of dense gas tracers in the CO-selected cores. As shown in Figure 5(b), the distributions of RMS noises of sources with and without detection are similar with an excess for non-detection sources at the high noise end ($\text{rms} > 0.12 \text{ K}$). The fractions of high noises are 0.18 and 0.07 for sources with and without detection. Nevertheless, more than 80% CO-selected cores without detection have RMS noises as low as the ones with detection. To further check the influence of the large range of sensitivity on the detection, we have separated the observed sources into high- and low-sensitivity groups using the median RMS noise ($\sim 0.06 \text{ K}$) as a threshold. The detection rates for the high- and low-sensitivity groups are 38.7% and 40.5%, respectively. Such consistency, together with the similarity between distributions of RMS noises of sources with and without detection, suggests that the detection of HCO^+ and/or HCN is not sensitivity limited.

4.1. Kinematics

We have carefully inspected the spectra of sources with detection in HCO^+ and/or HCN to find that all targets show single-peaked profiles except for seven ones showing self-absorption features (see Figure 3). Among the seven exceptions, two are red profiles (i.e. lines with higher peaks skewed to the red sides; G084.79-01.11A1 and G120.16+03.09A1) and four blue profiles (G114.56+14.72A1, G126.49-01.30A2, G172.85+02.27A1, and G226.36-0-0.50A1). The other one shows symmetric double-peaked profile with a dip at the line center (G120.98+02.66A1). Asymmetric double-peaked profiles are always regarded as effective tracers of kinematics in star-forming cores with blue profiles linked to inward motions (e.g., collapse or infall, Zhou et al. 1993; Wu & Evans 2003; Evans et al. 2005; Wu et al. 2005) and red profiles for outward motions (e.g., outflow or expansion Wu et al. 2007;

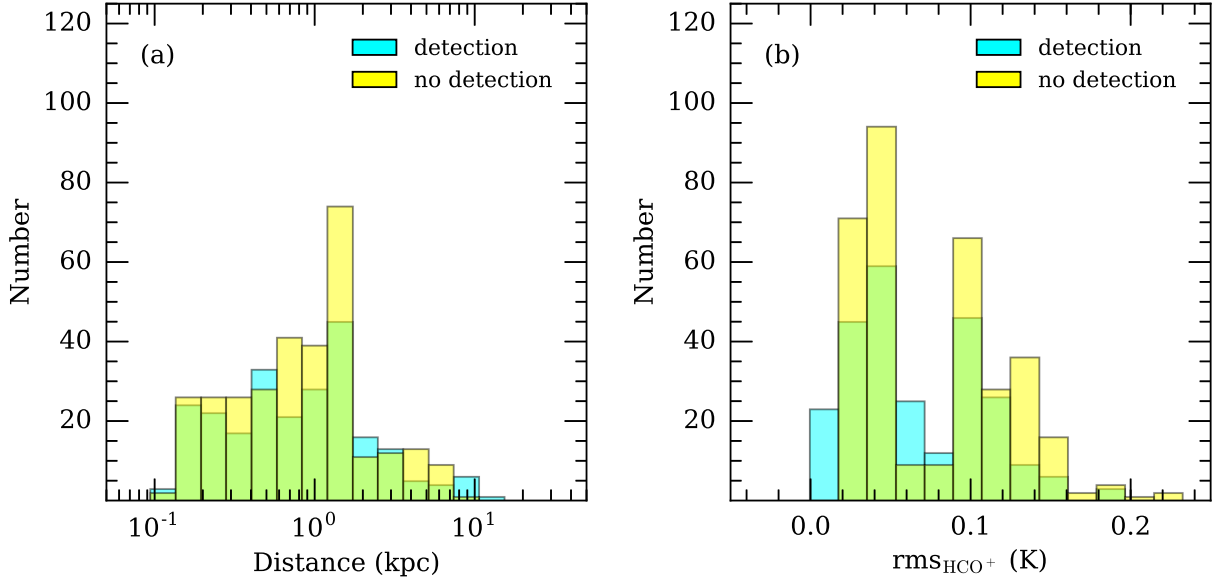


Figure 5. Distributions of distances (a) and RMS noise of HCO^+ (b) for sources with detection (cyan) in ether HCO^+ or HCN , and sources without detection (yellow) in neither HCO^+ nor HCN . The green means an overlay between the two groups.

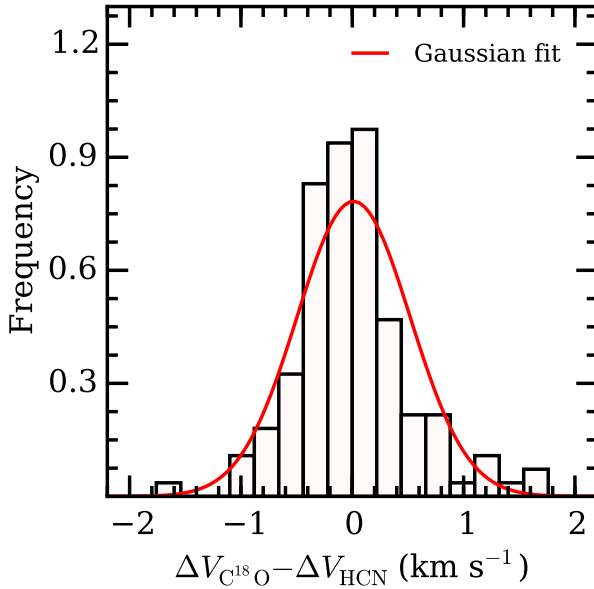


Figure 6. Distributions between differences of line widths of C^{18}O and HCN .

[Yuan et al. 2013](#)). The detection rates of blue and red profiles are 1.2% and 0.8%, significantly smaller than the values in surveys toward low- and high-mass star-forming regions. Based on results in the literature, [Evans \(2003\)](#) found the detection rates of blue (red) profiles in Class -I, 0, and I low-mass star-forming regions are 35% (6%), 33% (5%), and 50% (19%), respectively. Among the 48 high-mass clumps mapped in $\text{HCN } J = 3 - 2$ and an optically thin line ($\text{H}^{13}\text{CN } J = 3 - 2$ or $\text{C}^{34}\text{S } J = 5 - 4$), [Wu et al. \(2010\)](#) reported detection rates of 44% and 31% for blue and red profiles. We note that the difference between detection rates of asymmetric profiles in this work and that in the literature are not due to a difference in S/N of the observations, because the detection rates are still significantly low (< 3%) even if we only consider sources with $S/N > 10$. The small detection rates of asymmetric double-peaked profiles in this work indicate

rareness of bulk-motions in these dense CO-selected cores, suggesting they are relatively quiescent compared to classical star-forming regions.

Another indicator of kinematics that can be extracted from single-point observations could be the line widths. The mean widths of ^{12}CO , ^{13}CO , and C^{18}O of the CO-selected cores with valid detection in HCO^+ and/or HCN are 2.95 , 1.67 , and 1.08 km s^{-1} , relatively larger than that in [Wu et al. \(2012\)](#) in which they are 2.0 , 1.3 , and 0.8 km s^{-1} . The spectra are also slightly wider than those of CO-selected cores in Orion (0.9 km s^{-1} for ^{13}CO), Taurus (1.8 km s^{-1} for ^{12}CO and 1.1 km s^{-1} for ^{13}CO), and California (2.2 km s^{-1} for ^{12}CO and 1.4 km s^{-1} for ^{13}CO) molecular complexes ([Liu et al. 2012](#); [Meng et al. 2013](#)). Slightly larger line widths detected in this work may be attributed to that the cores with detection in HCO^+ and/or HCN are significantly denser than those in Taurus, California and Orion complexes (see section 3.2) and higher ram pressures make additional contribution to the line widths. Another possibility could be that the CO-selected cores with detection in HCO^+ and/or HCN are more turbulent.

Using data of multiple lines from distinct species with significantly different critical densities, we can statistically examine the difference of kinematics in separate regions. Here, we mainly compare the line widths of C^{18}O and HCN which, in general, are optically thin. The typical source-averaged volume density is $4.6 \times 10^3 \text{ cm}^{-3}$ (see section 2), indicating that there may be a significant volume with density above 10^4 cm^{-3} in these sources. With a critical density no larger than 10^4 cm^{-3} , $\text{C}^{18}\text{O } J = 1 - 0$ mainly originates from the exterior of a core. Meanwhile, $\text{HCN } J = 1 - 0$ is a good tracer of the inner region due to its significantly higher critical density of $> 10^5 \text{ cm}^{-3}$. The line widths of C^{18}O are in the range of 0.17 – 3.39 km s^{-1} with a mean value of 1.08 km s^{-1} , while those of HCN ranging from 0.69 to 2.70 km s^{-1} with a mean of 1.06 . The typical optical depths are 0.2 and 0.3 for $\text{C}^{18}\text{O } J = 1 - 0$ and $\text{HCN } J = 1 - 0$, respectively. Such small optical depths can only broaden the line widths by a factor of < 10% which has been estimated using Equation 3 of [Phillips et al. \(1979\)](#). We note that the minimum

value for HCN is only an upper limit due to the poor spectral resolution of our observations (see section 2). The mean widths of C¹⁸O and HCN are almost equal to each other. The distribution of difference between line widths of C¹⁸O and HCN, which can be fitted using a Gaussian with a $\mu = 0.01$ km s⁻¹ and a $\sigma = 0.51$ km s⁻¹, is shown in Figure 6. Intriguingly, the width difference is very small with statistical significance. This is contrary to the results in Wu et al. (2010) in which larger widths of transitions with higher critical densities are treated as an indication of larger turbulence in the inner region of dense cores. The almost equivalence between widths of C¹⁸O and HCN suggests that the inner regions of CO-selected cores are not more turbulent than the exterior, different from the situation in high-mass star-forming cores where the interior is of larger turbulence (e.g., Wu et al. 2010; Garay et al. 2015). Compared to the two optically thin lines (i.e., C¹⁸O $J = 1 - 0$ and HCN $J = 1 - 0$), the lines of ¹³CO $J = 1 - 0$ are relatively broader with widths ranging from 0.59 to 6.25 km s⁻¹ with a mean value of 1.67 . The typical difference between line widths of ¹³CO and HCN is 0.65 km s⁻¹, and the value is 0.42 km s⁻¹ even accounting for the broadening attributed to optical depth. This indicates the surrounding clouds are more turbulent.

4.2. Coupling of Different Species

In the survey toward 674 *Planck* cold clumps, Wu et al. (2012) found that the central velocities of transitions from CO and its isotopologues are strikingly consistent with each other. This feature could be reasonable in quiescent regions, for CO and its isotopologues should be well coupled with each other without active disturbance. In this work correlations among central velocities of ¹³CO, HCO⁺ and HCN, which are shown in Figure 7, have been examined. The differences of central velocities between ¹³CO and HCO⁺ ($V_{^{13}\text{CO}} - V_{\text{HCO}^+}$), ¹³CO and HCN ($V_{^{13}\text{CO}} - V_{\text{HCN}}$), HCO⁺ and HCN ($V_{\text{HCO}^+} - V_{\text{HCN}}$) have mean values of 0.006 ± 0.4 , 0.05 ± 0.4 , 0.002 ± 0.6 km s⁻¹. Intriguingly, the differences are strikingly small, which may be an indication of quiescent features for these CO-selected cores. Noticeably, the deviations of ($V_{^{13}\text{CO}} - V_{\text{HCO}^+}$), ($V_{^{13}\text{CO}} - V_{\text{HCN}}$), and ($V_{\text{HCO}^+} - V_{\text{HCN}}$) from zero seems to be consistent with the critical densities of the $J = 1 - 0$ transitions of ¹³CO ($\sim 10^3$ cm⁻³), HCO⁺ ($\sim 7 \times 10^4$ cm⁻³), and HCN ($\sim 5 \times 10^5$ cm⁻³). If HCN, HCO⁺, and ¹³CO trace gases from the interior to the exterior, the deviation of velocity difference from zero can also reflect the spatial correlation among different species. For instance, the small deviation of ($V_{\text{HCO}^+} - V_{\text{HCN}}$) may indicate that HCO⁺ is better coupled with HCN than CO.

Shown in Figure 8 are relations of velocity integrated intensities of ¹²CO, ¹³CO, C¹⁸O, and HCO⁺ with that of HCN. The intensities of CO and its isotopologues seem not correlated with that of HCN. However, the relationship between HCO⁺ and HCN follows a power law of $W_{\text{HCO}^+} = 2.3 \times W_{\text{HCN}}^{0.8}$ with a coefficient of determination of $R^2 = 0.7$ indicating about 70% of the data points can be well represented by the fitted linear relation in the log-log space. Such prominent correlation gives additional evidence to the coupling between HCO⁺ and HCN. Strong correlation between HCO⁺ and HCN was also detected in Liu et al. (2013b) and interpreted as an indicator of a tight chemical connection.

4.3. Abundances of HCO⁺ and HCN

The statistics of column densities and fractional abundances of HCO⁺ and HCN are given in Table 3. The column densities

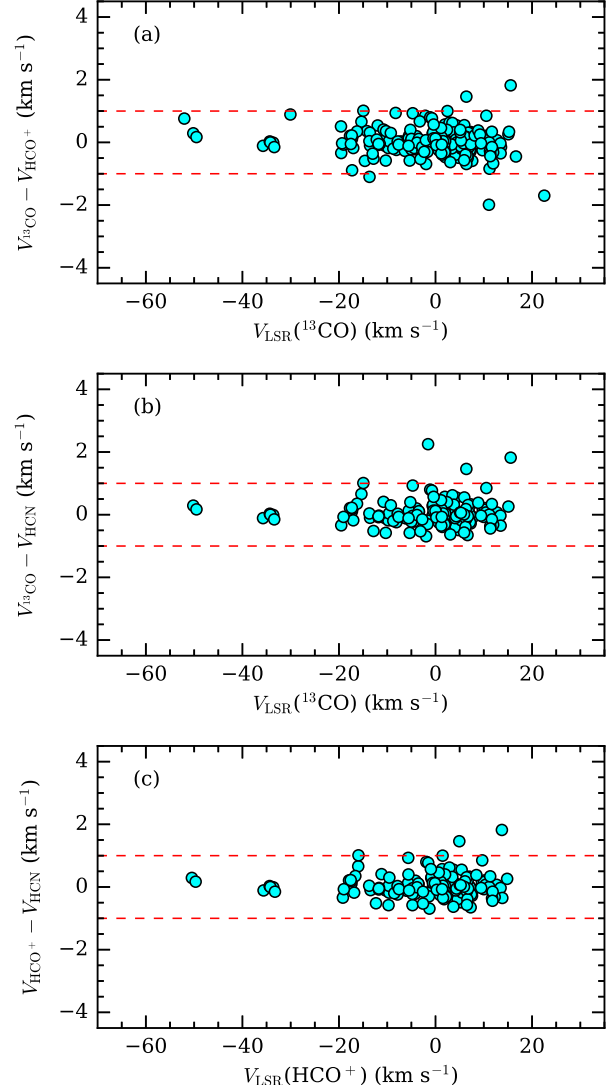


Figure 7. Correlations among velocity centroids of different species. (a) $V_{\text{LSR}}(\text{HCO}^+)$ vs. $V_{\text{LSR}}(^{13}\text{CO})$; (b) $V_{\text{LSR}}(\text{HCN})$ vs. $V_{\text{LSR}}(^{13}\text{CO})$; (c) $V_{\text{LSR}}(\text{HCN})$ vs. $V_{\text{LSR}}(\text{HCO}^+)$. The lower panels shows the velocity differences.

of HCO⁺ are in the range of $(0.07 - 24.16) \times 10^{12}$ cm⁻² with a mean value of 1.69×10^{12} cm⁻² , while that of HCN ranging from 0.24×10^{12} cm⁻² to 16.15×10^{12} cm⁻² with a mean of 1.57×10^{12} cm⁻². The abundances of HCO⁺ (HCN) range from 3.0×10^{-12} (1.3×10^{-11}) to 1.5×10^{-9} (5.6×10^{-10}) with a mean value of 1.5×10^{-10} (1.4×10^{-10}) which are significantly lower than values in low- to high-mass star-forming regions where the abundances of both HCO⁺ and HCN are in the range of $10^{-10} - 10^{-8}$ (Dutrey et al. 1997; Hirota et al. 1998; Vasyunina et al. 2011; Sanhueza et al. 2012; Liu et al. 2013b; Gerner et al. 2014; Miettinen 2014). The low abundances in this work could be attributed to poor spatial resolutions of our observations which have led to severe effect of beam dilution. The CO-selected cores with valid detection in HCO⁺ and/or HCN have distances ranging from 0.1 pc to 14.7 kpc with a mean of 1.4 kpc. The corresponding physical scales covered by one beam range from 0.03 pc to 4.3 pc with a mean of 0.35 pc. However the region where the gas is dense enough for HCO⁺ and HCN to be detectable would be smaller than 0.1 pc. Thus the measured column densities of HCO⁺ and HCN have been severely diluted by a factor of tens on aver-

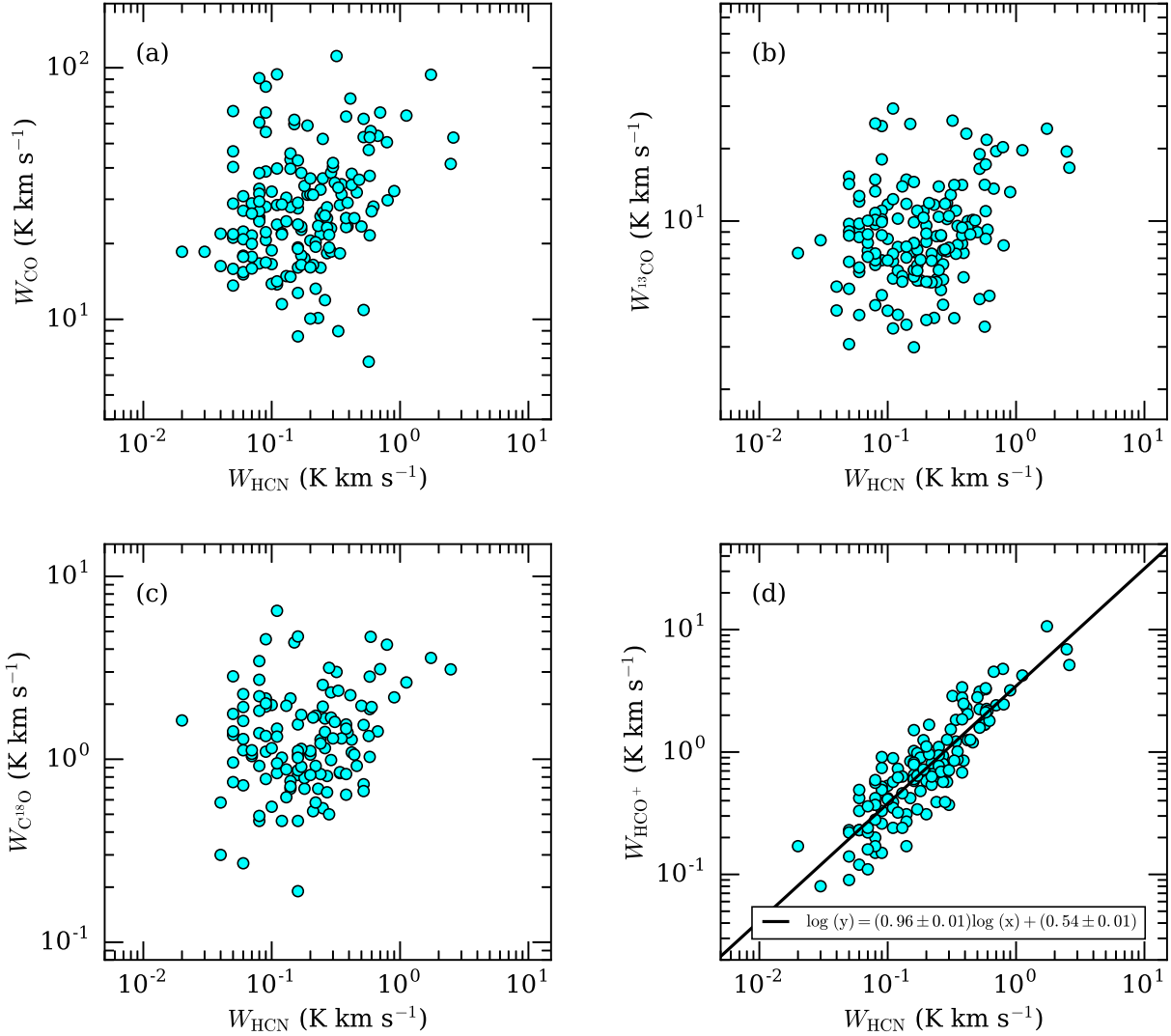


Figure 8. Velocity integrated intensities of CO (a), ^{13}CO (b), C^{18}O (c), and HCO^+ (d) as functions of that of HCN.

age, even by a factor of 10^3 for the farthest sources. We note that the H_2 column densities, which have been used to obtain fractional abundances of HCO^+ and HCN, were estimated based on CO observations. As aforementioned, the variation of $[\text{C}^{12}/\text{C}^{13}]$, $[\text{O}^{16}/\text{O}^{18}]$ and $[\text{CO}]/[\text{H}_2]$ ratios would lead to large uncertainties to the results. Further dust observations with sufficient resolution are needed to better constrain the abundances.

4.4. PGCCs with Dense Gas

As the first survey of dense gas towards *Planck* cold clumps, the statistical results in this work may lead us to determine whether there are any hints, in the many physical parameters given in the PGCC catalog, that can point to the presence of dense gas.

For sources detected in dense gas tracers, what makes them stand out of the rest? To address this question, we have examined some parameters from CO observations i.e., peak intensities of ^{13}CO , line widths of ^{13}CO , H_2 column densities, and excitation temperatures of CO. Shown in Figure 9 are histograms of these inspected parameters. The CO-selected cores with and without detection in HCO^+ and/or HCN share common distributions for line widths of ^{13}CO . The peak inten-

sities of ^{13}CO and excitation temperatures of CO for sources detected in HCO^+ and/or HCN are systematically higher than that of sources without detection. For H_2 column densities, the two groups of sources share a similar distribution at low-to intermediate densities. There is a prominent excess at H_2 column densities higher than $2 \times 10^{22} \text{ cm}^{-2}$ for sources detected in dense gas tracers. In general, sources detected in HCO^+ and/or HCN would have higher CO excitation temperatures and, probably, higher column densities compared to the ones without detection.

In order to pinpoint which parameter(s) given in the PGCC catalog can point to the presence of dense gas, we have revisited H_2 column densities, dust temperatures, masses and luminosities of all PGCCs (black) and the ones consisting CO-selected cores with (red) and without (blue) detection in HCO^+ and/or HCN. The histograms and statistics of these parameters are presented in Figure 10 and Table 4. In general, the PGCCs containing CO-selected cores (for both with and without detection in dense gas tracers) are denser and colder compared to the whole PGCC sample. There is no surprise for this point because the CO-selected cores were identified from ECCs which constitute the high-S/N and cold tail of PGCC objects. PGCCs containing CO-selected cores detected in

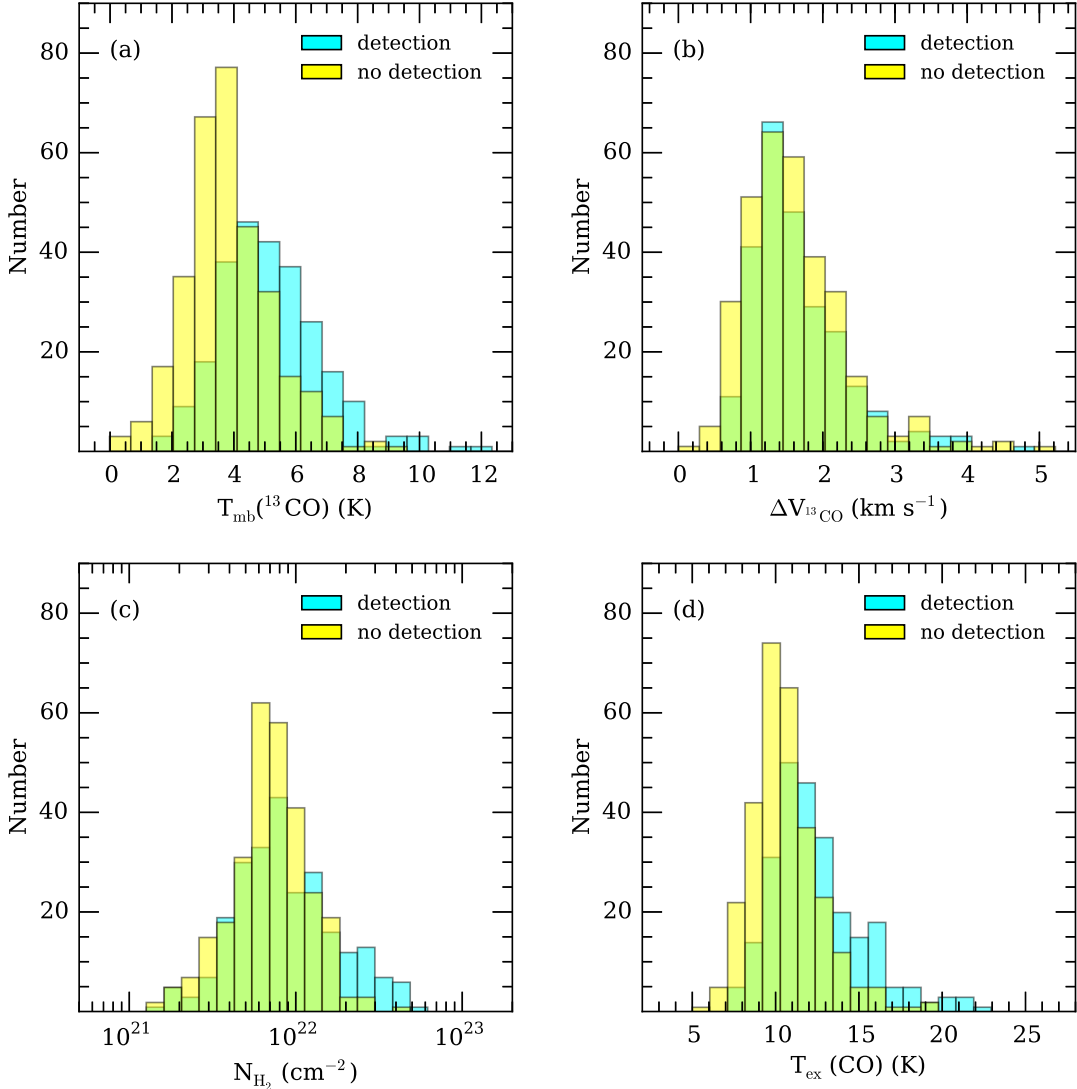


Figure 9. Distributions of velocity-integrated intensities of ^{13}CO (a), line widths of ^{13}CO (b), H_2 column densities and excitation temperatures of CO for sources with detection (cyan) in ether HCO^+ or HCN, and sources without detection (yellow) in neither HCO^+ nor HCN. The green means an overlay between the two groups.

HCO^+ and/or HCN are slightly denser compared to the ones with no detection. There is no significant difference between distributions of dust temperatures for these two subsamples. As shown in Figure 10(c), the clump masses of the full PGCC sample and the PGCCs without detection in dense gas have similar distributions, while that of the PGCCs with detection in HCO^+ and/or HCN slightly deviating to the high mass end with larger median values. For luminosities, the full PGCC sample and the other two subsamples share similar distributions and the median values are also consistent in a factor of one (see Figure 10 and Table 4). Although there are no significant differences for parameters among distinct samples, we still tentatively found that PGCC sources containing dense gas would be denser and more massive compared to the remaining pool. On the basis of the statistics presented in Table 4, we tentatively estimate that there may be about 1000 PGCC objects having sufficient reservoir of dense gas to form stars.

5. CONCLUSIONS

We have carried out single-pointing observations in the $J = 1 - 0$ transitions of HCO^+ and HCN towards 621 CO-selected molecular cores associated with *Planck* cold clumps. Among them, 250 sources have valid detection in either HCO^+ and/or HCN, including 138 cores detected in both lines, 92 cores only in HCO^+ , and 20 cores only in HCN. Spectra of the $J = 1 - 0$ transitions of ^{12}CO , ^{13}CO , and C^{18}O for the 250 cores were extracted from previous mapping observations to construct a multi-line data set to reveal some kinematic and chemical properties.

Spectra of $\text{HCO}^+ J = 1 - 0$ and HCN $J = 1 - 0$ of all sources show single-peaked profiles except for seven ones showing self-absorption features. Among the seven exceptions, two are red profiles, four blue profiles. The other one shows a symmetric double-peaked profile with a dip at the line center. The low detection rate of asymmetric profiles suggests the CO-selected cores are more quiescent compared to classical star-forming regions.

The difference between line widths of C^{18}O and HCN are close to zero with a small standard deviation, indicating that the inner regions of CO-selected cores are not more turbu-

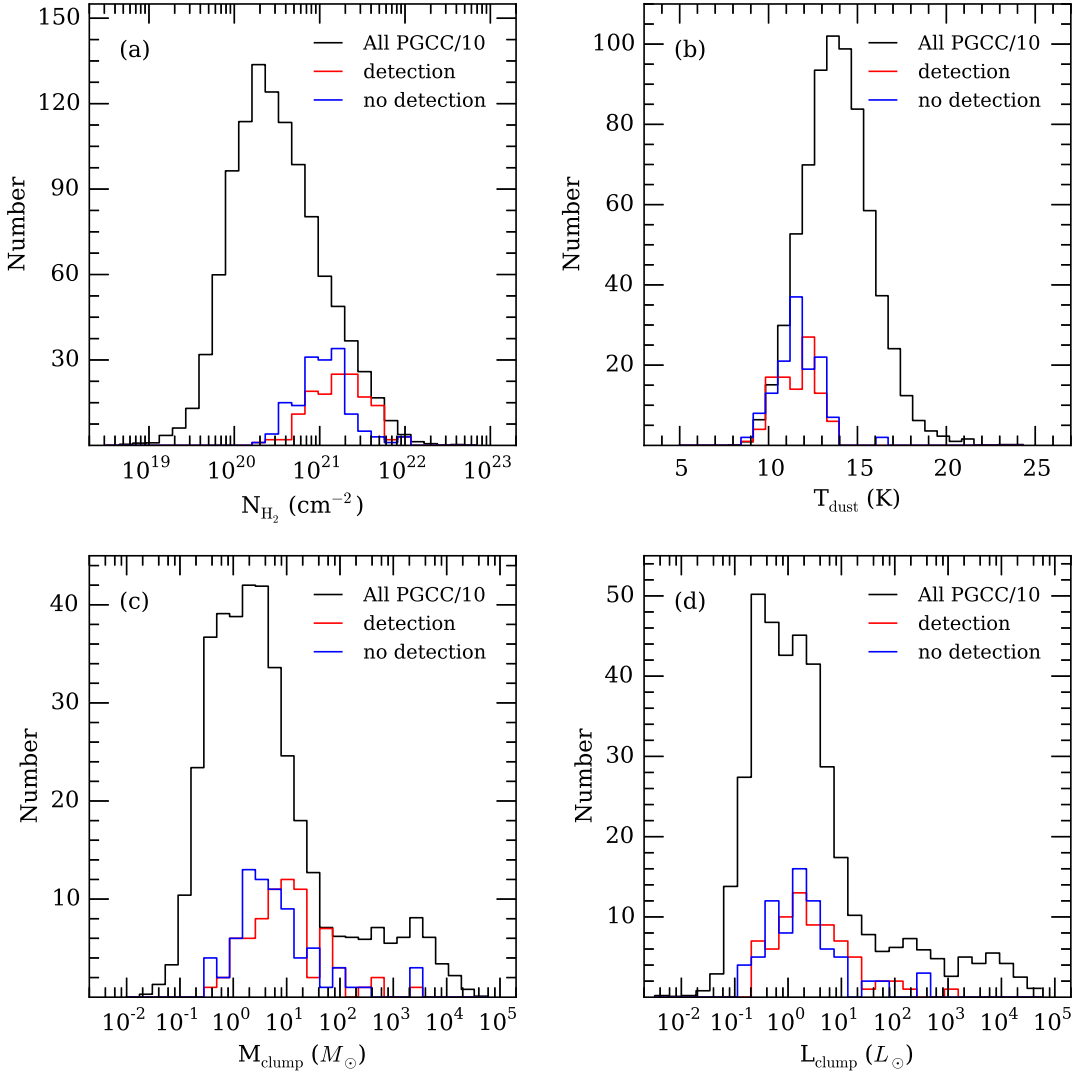


Figure 10. Distributions of H_2 column densities, dust temperatures, masses and luminosities of all PGCCs (black) and the ones consisting CO-selected cores with (red) and without (blue) detection in HCO^+ and/or HCN . We note that all the parameters are from the PGCC catalog (Planck Collaboration et al. 2015)

lent than the exterior. This is different from the situation in high-mass star-forming cores where the interior is of larger turbulence (Wu et al. 2010; Garay et al. 2015).

The central velocities of HCO^+ are more consistent with that of HCN than ^{13}CO . The velocity-integrated intensities of HCO^+ are well correlated with that of HCN . These features indicate that gaseous HCO^+ is better coupled with HCN than CO and its isotopologues.

The H_2 column densities of sources with detection in HCO^+ or HCN have been deduced from spectra of C^{18}O or ^{13}CO , and are in the range of $(1.5 - 70.9) \times 10^{21} \text{ cm}^{-2}$ with a mean value of $1.3 \times 10^{22} \text{ cm}^{-2}$, significantly higher than those of CO-selected cores in Orion, Taurus, Perseus, and California complexes.

The estimated fractional abundances of HCO^+ (HCN) range from 3.0×10^{-12} (1.3×10^{-11}) to 1.5×10^{-9} (5.6×10^{-10}) with a mean value of 1.5×10^{-10} (1.4×10^{-10}) which are significantly lower than values in low- to high-mass star-forming regions. The low abundances detected in this work may be attributed to beam dilution.

The inspection of some parameters from CO observations suggests that CO-selected cores detected in HCO^+ and/or

HCN would have higher CO excitation temperatures and, probably, higher column densities compared to the ones without detection. Among the parameters given in the PGCC catalog, we found that the H_2 column density would serve as an indicator of the presence of dense gas in PGCCs. On the basis of the inspection of the parameters given in the PGCC catalog, we suggest that there are about 1 000 PGCC objects may have sufficient reservoir of dense gas to form stars.

This work is supported by the National Natural Science Foundation of China through grants of 11503035, 11573036, 11373009, 11433008 and 11403040, the China Ministry of Science and Technology under State Key Development Program for Basic Research through the grant of 2012CB821800, the International S&T Cooperation Program of China through the grand of 2010DFA02710, the Beijing Natural Science Foundation through the grant of 1144015, and the Young Researcher Grant of National Astronomical Observatories, Chinese Academy of Sciences. KW acknowledges support from the ESO fellowship and grant WA3628-1/1 through the DFG priority programme 1573 ‘Physics of the Interstellar Medium’ (<http://www.ism-spp.de>). We give our thanks to the staff at

the Qinghai Station of Purple Mountain Observatory for their hospitable assistance during the observations and the Key Laboratory for Radio Astronomy of Chinese Academy of Sciences for partial support in the operation of the telescope.

REFERENCES

- Aguirre, J. E., Ginsburg, A. G., Dunham, M. K., et al. 2011, ApJS, 192, 4 [1](#)
- André, P., Men'shchikov, A., Bontemps, S., et al. 2010, A&A, 518, L102 [1](#)
- Boger, G. I., & Sternberg, A. 2005, ApJ, 632, 302
- Dutrey, A., Guilloteau, S., & Guelin, M. 1997, A&A, 317, L55 [4.3](#)
- Evans, N., II 2003, SFChem 2002: Chemistry as a Diagnostic of Star Formation, 157 [4.1](#)
- Evans, N. J., II, Lee, J.-E., Rawlings, J. M. C., & Choi, M. 2005, ApJ, 626, 919 [4.1](#)
- Fontani, F., Giannetti, A., Beltrán, M. T., et al. 2012, MNRAS, 423, 2342 [3.2](#)
- Garay, G., Mardones, D., Contreras, Y., et al. 2015, ApJ, 799, 75 [4.1, 5](#)
- Gerner, T., Beuther, H., Semenov, D., et al. 2014, A&A, 563, A97 [4.3](#)
- Hatchell, J., Thompson, M. A., Millar, T. J., & MacDonald, G. H. 1998, A&AS, 133, 29 [3.2](#)
- Herbst, E. 1978, ApJ, 222, 508
- Herbst, E., & Klemperer, W. 1973, ApJ, 185, 505
- Hirota, T., Yamamoto, S., Mikami, H., & Ohishi, M. 1998, ApJ, 503, 717 [4.3](#)
- Hou, L. G., & Han, J. L. 2014, A&A, 569, A125 [2](#)
- Juvela, M., Ristorcelli, I., Marshall, D. J., et al. 2015, arXiv:1501.07092 [1](#)
- Juvela, M., Ristorcelli, I., Montier, L. A., et al. 2010, A&A, 518, L93 [1](#)
- Juvela, M., Ristorcelli, I., Pagani, L., et al. 2012, A&A, 541, A12 [1](#)
- Juvela, M., Ristorcelli, I., Pelkonen, V.-M., et al. 2011, A&A, 527, A111 [1](#)
- Liu, T., Wu, Y., & Zhang, H. 2012, ApJS, 202, 4 [1, 2, 3.2, 4.1](#)
- Liu, T., Wu, Y., Mardones, D., et al. 2015, PKAS, 30, 79 [1](#)
- Liu, T., Wu, Y., & Zhang, H. 2013a, ApJ, 775, L2 [1](#)
- Liu, X.-L., Wang, J.-J., & Xu, J.-L. 2013b, MNRAS, 431, 27 [4.2, 4.3](#)
- Maret, S., Bergin, E. A., & Tafalla, M. 2013, A&A, 559, A53
- McDowell, R. S. 1988, J. Chem. Phys., 88, 356 [3.2](#)
- Meng, F., Wu, Y., & Liu, T. 2013, ApJS, 209, 37 [1, 2, 3.2, 4.1](#)
- Miettinen, O. 2012, A&A, 540, A104 [3.2](#)
- Miettinen, O. 2014, A&A, 562, A3 [3.2, 4.3](#)
- Molinari, S., Swinyard, B., Bally, J., et al. 2010, PASP, 122, 314 [1](#)
- Parikka, A., Juvela, M., Pelkonen, V.-M., Malinen, J., & Harju, J. 2015, A&A, 577, A69 [1](#)
- Pety, J. 2005, SF2A-2005: Semaine de l'Astrophysique Francaise, 721 [2](#)
- Phillips, T. G., Huggins, P. J., Wannier, P. G., & Scoville, N. Z. 1979, ApJ, 231, 720 [4.1](#)
- Pineda, J. L., Langer, W. D., Velusamy, T., & Goldsmith, P. F. 2013, A&A, 554, A103 [3.2, 3.2](#)
- Planck Collaboration, Ade, P. A. R., Aghanim, N., et al. 2011a, A&A, 536, A1 [1](#)
- Planck Collaboration, Ade, P. A. R., Aghanim, N., et al. 2011b, A&A, 536, A7 [1](#)
- Planck Collaboration, Ade, P. A. R., Aghanim, N., et al. 2011c, A&A, 536, A22 [1](#)
- Planck Collaboration, Ade, P. A. R., Aghanim, N., et al. 2011d, A&A, 536, A23 [1, 3, 3.2](#)
- Planck Collaboration, Ade, P. A. R., Aghanim, N., et al. 2014, A&A, 571, A13 [1](#)
- Planck Collaboration, Ade, P. A. R., Aghanim, N., et al. 2015, arXiv:1502.01599 [1, 2, 10, 5](#)
- Sanhueza, P., Jackson, J. M., Foster, J. B., et al. 2012, ApJ, 756, 60 [4.3](#)
- Schuller, F., Menten, K. M., Contreras, Y., et al. 2009, A&A, 504, 415 [1](#)
- Shan W., Yang J., Shi S., et al. 2012, IEEE Transactions on Terahertz Science and Technology, 2, 593 [2](#)
- Tauber, J. A., Mandolesi, N., Puget, J.-L., et al. 2010, A&A, 520, A1 [1](#)
- Vasyunina, T., Linz, H., Henning, T., et al. 2011, A&A, 527, A88 [4.3](#)
- Wang, K., Wu, Y. F., Ran, L., Yu, W. T., & Miller, M. 2009, A&A, 507, 369 [1](#)
- Wang, K., Zhang, Q., Testi, L., et al. 2014, MNRAS, 439, 3275 [1](#)
- Wilson, T. L., & Rood, R. 1994, ARA&A, 32, 191 [3.2, 3.2](#)
- Wu, J., & Evans, N. J., II 2003, ApJ, 592, L79 [4.1](#)
- Wu, J., Evans, N. J., II, Shirley, Y. L., & Knez, C. 2010, ApJS, 188, 313 [4.1, 5](#)
- Wu, Y., Henkel, C., Xue, R., Guan, X., & Miller, M. 2007, ApJ, 669, L37 [4.1](#)
- Wu, Y., Liu, T., Meng, F., et al. 2012, ApJ, 756, 76 [1, 2, 3.2, 3.2, 4.1, 4.2](#)
- Wu, Y., Zhu, M., Wei, Y., et al. 2005, ApJ, 628, L57 [4.1](#)
- Yuan, J.-H., Wu, Y., Li, J. Z., Yu, W., & Miller, M. 2013, MNRAS, 429, 954 [4.1](#)
- Zhou, S., Evans, N. J., II, Koempe, C., & Walmsley, C. M. 1993, ApJ, 404, 232 [4.1](#)

Table 1
Observational Parameters of HCO^+ and HCN

Designation	R.A.	Dec.	$\text{HCO}^+ J = 1 - 0$						$\text{HCN } J = 1 - 0$					
			rms (K)	T_{mb} (K)	$\int T_{\text{mb}} dv$ (K km s $^{-1}$)	v_{lsr} (km s $^{-1}$)	FWHM (km s $^{-1}$)	rms (K)	T_{mb} (K)	$\int T_{\text{mb}} dv$ (K km s $^{-1}$)	v_{lsr} (km s $^{-1}$)	FWHM (km s $^{-1}$)	τ	
G026.45+08.02a1	18h11m20.92s	-2d00m22.7s	0.04	0.60(0.07)	0.39(0.03)	6.17(0.02)	0.60(0.05)	0.03	0.14(0.20)	0.11(0.17)	6.31(0.10)	1.10(0.19)	0.14(0.15)	
G031.26-05.37a1	19h07m39.03s	-4d00m27.3s	0.12	0.40(0.18)	0.27(0.09)	0.74(0.12)	0.64(0.20)	
G038.36-00.95a1	19h04m44.03s	4d22m51.4s	0.04	0.16(0.04)	0.34(0.05)	17.11(0.16)	1.98(0.36)	
G043.02+08.36a1	18h39m21.54s	12d41m35.3s	0.19	1.00(0.20)	0.44(0.12)	4.07(0.05)	0.41(1.72)	
G057.17+03.41a1	19h24m55.57s	23d04m21.7s	0.03	0.13(0.13)	0.07(0.02)	12.03(0.12)	0.54(0.50)	
G058.97-01.66b1	19h47m42.84s	22d06m07.8s	0.04	0.22(0.39)	0.10(0.03)	24.23(0.07)	0.41(0.71)	
G070.44-01.54a2	20h14m31.88s	31d57m05.5s	0.11	0.47(0.07)	2.30(0.22)	11.18(0.22)	4.61(0.51)	0.09	0.33(0.82)	0.41(1.04)	9.53(0.19)	1.67(0.50)	0.10(0.16)	
G070.72-00.63a1	20h11m59.82s	32d42m02.8s	0.03	0.11(0.03)	0.38(0.06)	13.06(0.27)	3.35(0.67)	
G074.11+00.11a1	20h17m56.73s	35d56m42.8s	0.03	0.16(1.34)	0.07(0.02)	-0.88(0.05)	0.41(3.44)	
G084.79-01.11a1	20h57m10.57s	43d46m28.0s	0.03	1.08(0.05)	2.87(0.08)	1.36(0.02)	2.50(0.08)	0.03	0.24(0.07)	0.32(0.10)	1.48(0.04)	1.79(0.09)	0.74(0.16)	
G084.79-01.11a2	20h56m51.94s	43d44m15.2s	0.03	0.26(0.03)	0.89(0.07)	0.90(0.11)	3.21(0.27)	0.03	0.09(0.09)	0.11(0.11)	0.90(0.12)	1.65(0.25)	1.17(0.87)	
G084.79-01.11a3	20h56m42.28s	43d40m42.4s	0.03	0.13(0.02)	0.33(0.04)	0.67(0.15)	2.35(0.35)	0.02	0.06(0.18)	0.09(0.26)	0.68(0.29)	1.93(0.55)	0.23(0.47)	
G084.79-01.11a4	20h56m45.19s	43d37m17.7s	0.04	0.36(0.06)	0.37(0.04)	6.53(0.05)	0.97(0.12)	0.03	0.12(0.17)	0.08(0.08)	6.46(0.08)	0.93(0.13)	0.89(0.61)	
G089.93-02.16b1	21h20m02.04s	46d38m08.8s	0.09	0.30(0.09)	0.35(0.08)	1.66(0.13)	1.10(0.24)	0.05	0.11(0.17)	0.16(0.24)	2.11(0.31)	1.81(0.51)	0.10(0.14)
G089.93-01.94a1	21h19m48.94s	46d53m07.6s	0.09	0.30(0.09)	0.35(0.08)	1.66(0.13)	1.10(0.24)	0.05	0.11(0.17)	0.16(0.24)	2.11(0.31)	1.81(0.51)	0.10(0.14)
G093.12-10.40a2	22h04m51.19s	42d36m55.4s	0.03	0.06(0.13)	0.04(0.08)	-0.62(0.15)	0.86(0.24)	0.10(0.15)	
G093.44-04.66a1	21h45m44.03s	47d11m25.2s	0.10	0.19(0.44)	0.10(0.24)	7.76(0.15)	0.69(0.47)	0.10(0.14)	
G093.44-04.66a2	21h46m01.88s	47d11m06.1s	0.06	0.69(0.10)	0.75(0.07)	5.26(0.04)	1.02(0.12)	0.06	0.34(0.26)	0.26(0.20)	5.09(0.06)	1.03(0.14)	0.33(0.20)	
G093.62-04.44a1	21h45m41.91s	47d33m11.9s	0.06	0.58(0.09)	0.73(0.07)	3.69(0.05)	1.20(0.14)	0.05	0.23(0.12)	0.12(0.17)	0.69(0.17)	0.59(0.24)	0.10(0.47)	
G093.75-04.59a1	21h47m08.74s	47d31m10.0s	0.09	0.35(0.15)	0.39(0.10)	3.67(0.14)	1.05(0.35)	0.08	0.25(1.83)	0.24(0.79)	3.47(0.14)	1.30(0.27)	0.10(0.47)	
G093.91+1.02a2	20h37m09.60s	57d40m28.8s	0.03	0.15(1.12)	0.07(0.02)	-1.26(0.05)	0.41(3.06)	
G096.37+0.29a1	20h45m39.78s	59d50m01.0s	0.03	0.12(1.82)	0.05(0.02)	-6.45(0.07)	0.41(6.20)	
G097.09+10.12a1	20h51m07.82s	60d01m48.9s	0.03	0.20(0.92)	0.09(0.02)	-2.98(0.05)	0.41(1.89)	
G097.77+08.59a2	21h04m41.80s	59d52m59.3s	0.03	0.10(0.05)	0.10(0.03)	3.20(0.15)	0.93(0.40)	
G098.50-03.24a1	22h04m55.16s	51d31m08.1s	0.08	0.30(0.13)	0.48(0.12)	-5.98(0.16)	1.53(0.53)	0.07	0.35(0.11)	0.18(0.11)	-5.87(0.05)	0.69(0.37)	0.22(0.05)	
G098.96+13.68a1	20h36m12.76s	63d52m30.1s	0.03	0.21(0.05)	0.17(0.03)	-2.56(0.06)	0.75(0.14)	
G100.34+15.96a2	20h55m43.46s	67d45m18.7s	0.04	0.17(0.18)	0.09(0.02)	2.44(0.09)	0.51(0.54)	0.03	0.08(0.13)	0.05(0.08)	2.54(0.10)	0.82(0.16)	0.10(0.10)	
G102.72+15.36a1	20h42m50.57s	67d45m43.3s	0.03	0.16(0.07)	0.18(0.04)	1.47(0.09)	1.07(0.43)	
G102.72+15.36a2	20h43m26.12s	67d51m59.3s	0.03	0.09(0.04)	0.09(0.03)	2.50(0.14)	0.89(0.26)	
G102.72-25.98a1	23h24m08.29s	33d25m54.4s	0.03	0.11(0.94)	0.05(0.02)	-7.23(0.15)	0.41(3.49)	
G103.22-21.23a1	23h04m44.47s	43d30m52.2s	0.03	0.11(0.08)	0.05(0.03)	3.64(0.18)	0.45(0.19)	
G103.90+13.97a1	21h02m19.84s	67d55m00.5s	0.03	0.11(0.06)	0.09(0.03)	2.27(0.13)	0.76(0.32)	
G104.78+11.49a1	21h27m39.11s	66d53m46.3s	0.03	0.39(0.06)	0.26(0.03)	-9.41(0.04)	0.63(0.07)	0.03	0.14(0.14)	0.09(0.09)	-9.44(0.07)	0.86(0.14)	0.10(0.06)	
G105.55+0.40a1	21h41m03.61s	66d35m17.5s	0.03	0.25(0.03)	0.35(0.03)	-10.32(0.07)	1.31(0.13)	0.03	0.08(0.63)	0.11(0.82)	-10.36(0.21)	1.73(0.35)	0.10(0.49)	
G106.30+13.57a1	21h22m37.63s	69d22m32.9s	0.03	0.21(0.25)	0.30(0.30)	-9.76(0.33)	1.32(0.82)	
G108.85-00.80a1	22h58m40.27s	58d56m07.2s	0.14	0.66(0.11)	2.41(0.25)	-50.47(0.18)	3.45(0.43)	0.12	0.46(0.80)	0.70(1.22)	-50.40(0.14)	2.02(0.28)	0.10(0.11)	
G108.85-00.80a2	22h58m19.24s	58d57m55.3s	0.18	1.23(0.14)	4.22(0.32)	-49.69(0.12)	3.23(0.28)	0.15	0.55(0.36)	1.12(0.74)	-49.81(0.17)	2.70(0.25)	0.10(0.04)	
G110.65+09.65a1	22h28m17.01s	69d01m35.1s	0.03	0.34(0.04)	0.53(0.04)	-4.25(0.05)	1.49(0.13)	0.03	0.13(0.11)	0.10(0.09)	-4.31(0.09)	1.00(0.20)	0.31(0.19)	
G111.33+19.94a2	20h56m52.33s	77d12m33.1s	0.03	0.12(0.04)	0.21(0.04)	-7.16(0.18)	1.67(0.46)	
G111.66+20.20a1	20h57m21.72s	77d35m12.9s	0.03	0.20(0.03)	0.42(0.04)	-7.80(0.11)	2.00(0.20)	0.03	0.10(0.15)	0.10(0.16)	-7.47(0.12)	1.43(0.32)	0.16(0.17)	
G112.77+20.26a1	20h57m34.44s	0.04	0.28(0.03)	0.52(0.04)	-7.87(0.07)	1.73(0.16)	0.03	0.13(0.17)	0.09(0.12)	-7.62(0.07)	0.91(0.20)	0.30(0.29)		
G112.60+08.53a1	22h53m26.96s	68d53m41.17s	0.02	0.07(0.03)	0.14(0.03)	-5.71(0.25)	1.99(0.64)	
G113.42+6.97a1	21h59m28.92s	76d35m17.3s	0.02	0.07(0.02)	0.09(0.02)	-6.29(0.18)	1.31(0.35)	
G113.62+15.01a1	22h21m51.80s	75d03m17.3s	0.02	0.16(0.03)	0.17(0.02)	-5.65(0.06)	1.00(0.15)	0.02	0.04(0.03)	0.02(0.02)	-5.42(0.07)	0.69(0.06)	3.17(1.83)	
G114.56+14.72a1	22h35m35.60s	75d17m00.9s	0.04	0.23(0.04)	0.49(0.05)	-4.88(0.10)	2.02(0.23)	0.03	0.08(0.26)	0.09(0.31)	-4.93(0.23)	1.56(0.39)	0.10(0.21)	
G114.67+14.47a1	22h38m50.73s	75d11m45.1s	0.04	0.85(0.05)	1.10(0.04)	-4.16(0.02)	1.22(0.05)	0.03	0.32(1.16)	0.25(0.92)	-4.17(0.04)	1.05(0.06)	0.10(0.23)	
G115.81-03.54a1	23h36m47.86s	58d33m36.2s	0.08	0.63(0.12)	0.69(0.08)	-1.59(0.06)	0.13(0.16)	0.06	0.45(0.55)	0.26(0.32)	-0.76(0.08)	0.76(0.24)	0.12(0.09)	
G115.92+09.46a1	23h24m00.22s	71d08m22.0s	0.04	0.21(0.26)	0.09(0.02)	-3.93(0.06)	0.41(0.49)	
G117.11+12.42a1	23h24m53.70s	74d15m02.0s	0.04	0.20(0.04)	0.23(0.03)	-5.65(0.06)	1.00(0.15)	0.03	0.09(0.11)	0.06(0.08)	3.76(0.11)	0.94(0.26)	0.54(0.53)	
G120.16+03.09a1	0h24m25.75s	65d49m49.2s	0.16	1.45(0.12)	4.78(0.27)	-19.19(0.09)	3.11(0.19)	0.14	0.57(0.38)	0.79(0.53)	-19.37(0.08)	1.84(0.20)	0.59(0.30)	
G120.67+02.66a1	0h28m45.78s	65d27m15.7s	0.11	3.38(0.11)	3.38(0.17)	-17.42(0.05)	2.31(0.15)	0.09	0.34(0.21)	0.38(0.25)	-17.54(0.14)	1.51(0.28)	0.10(0.04)	
G120.67+02.66a2	0h29m43.72s	65d26m29.8s	0.15	1.62(0.12)	4.53(0.22)	-17.92(0.06)	2.63(0.14)	0.13	0.53(0.67)	0.67(0.86)	-17.54(0.10)	1.69(0.28)	0.21(0.20)	
G120.98+02.66a1	0h32m25.56s	65d27m37.7s	0.15	1.25(0.12)	3.26(0.22)	-17.39(0.09)	2.45(0.17)	0.14	0.48(0.44)	0.58(0.55)	-17.39(0.11)	1.62(0.30)	0.37(0.26)	

Table 1 — *Continued*

Designation	R.A.	Dec.	HCO ⁺ $J = 1 - 0$						HCN $J = 1 - 0$					
			rms (K)	T_{mb} (K)	$\int T_{\text{mb}} dv$ (K km s ⁻¹)	ν_{lsr} (km s ⁻¹)	FWHM (km s ⁻¹)	rms (K)	T_{mb} (K)	$\int T_{\text{mb}} dv$ (K km s ⁻¹)	ν_{lsr} (km s ⁻¹)	FWHM (km s ⁻¹)	τ	
G121.35+03.39b1	0h35m40.22s	66d14m18.0s	0.07	0.72(0.09)	0.84(0.07)	-5.68(0.04)	1.10(0.10)	0.06	0.25(0.24)	0.16(0.16)	-5.52(0.06)	0.87(0.13)	0.50(0.38)	
G122.01-07.48a2	0h45m01.77s	55d21m09.0s	0.03	0.12(0.06)	0.07(0.02)	-5.80(0.10)	0.52(0.20)	
G122.18-10.27a2	0h46m35.07s	52d34m57.4s	0.03	0.11(0.04)	0.11(0.03)	-10.40(0.14)	0.90(0.25)	
G125.66-00.55a1	1h15m45.75s	62d11m34.6s	0.06	0.64(0.06)	0.91(0.06)	-16.01(0.05)	1.34(0.10)	0.05	0.18(0.12)	0.09(0.08)	-15.80(0.08)	0.69(0.38)	0.77(0.41)	
G125.66-00.55a2	1h14m48.16s	62d11m34.6s	0.06	0.68(0.10)	0.92(0.08)	-14.04(0.06)	1.27(0.15)	
G125.66-00.55a2	1h14m48.16s	62d11m34.6s	0.06	0.47(0.12)	0.42(0.06)	-9.60(0.06)	0.83(0.17)	0.05	0.27(0.43)	0.15(0.25)	-9.46(0.08)	0.75(0.21)	0.31(0.39)	
G125.66-00.55b1	1h14m51.10s	62d10m14.8s	0.06	0.30(0.09)	0.38(0.07)	-9.68(0.10)	1.18(0.28)	0.05	0.16(0.10)	0.08(0.07)	-9.57(0.07)	0.69(0.37)	0.53(0.27)	
G126.27+05.11a1	1h26m30.08s	67d44m39.0s	0.16	0.35(0.54)	0.23(0.37)	-12.80(0.18)	0.87(0.35)	0.10(0.09)	
G126.49-01.30a1	1h21m10.05s	61d20m18.5s	0.07	0.74(0.09)	1.13(0.09)	-12.52(0.06)	1.44(0.13)	
G126.49-01.30a2	1h20m49.92s	61d27m02.8s	0.09	0.37(0.07)	1.25(0.16)	-12.33(0.21)	3.22(0.41)	0.10	0.34(0.38)	0.19(0.22)	-12.34(0.09)	0.76(0.22)	0.10(0.07)	
G128.95-00.18a1	1h43m34.22s	62d03m19.3s	0.13	0.61(0.17)	0.93(0.16)	-35.62(0.12)	1.43(0.32)	0.13	0.34(0.32)	0.27(0.26)	-35.91(0.15)	1.06(0.25)	0.10(0.06)	
G128.95-00.18a2	1h43m27.23s	61d58m54.1s	0.12	0.31(0.33)	0.17(0.21)	-43.70(0.15)	0.74(0.41)	0.10(0.12)	
G129.94+11.73a1	2h28m27.25s	0.02	0.08(0.04)	0.05(0.02)	-12.57(0.11)	0.55(0.20)	
G130.14+11.07a1	2h10m19.14s	72d37m27.7s	0.02	0.08(0.04)	0.07(0.02)	-14.57(0.12)	0.83(0.23)	
G131.72+09.70a1	2h40m10.77s	70d42m20.6s	0.04	0.12(0.06)	0.09(0.03)	-9.20(0.11)	0.69(0.28)	
G133.28+08.81a2	2h50m46.48s	69d14m29.2s	0.03	0.06(0.06)	0.04(0.04)	-21.94(0.19)	0.80(0.35)	0.10(0.05)		
G133.28+08.81b1	2h51m45.49s	69d14m32.8s	0.03	0.09(0.08)	0.05(0.04)	-16.46(0.09)	0.69(0.14)	0.10(0.05)		
G133.28+08.81b2	2h51m22.89s	69d13m10.2s	0.04	0.48(0.04)	0.71(0.04)	-11.18(0.04)	1.41(0.10)	0.03	0.21(0.67)	0.20(0.65)	-11.18(0.06)	1.28(0.13)	0.10(0.20)	
G133.48+09.02a1	2h54m32.60s	69d20m31.8s	0.04	0.24(0.03)	0.84(0.07)	-16.61(0.12)	3.22(0.33)	0.03	0.14(0.20)	0.15(0.22)	-16.78(0.09)	1.43(0.20)	0.10(0.09)	
G136.31-01.77a2	2h36m07.73s	58d20m23.2s	0.12	0.96(0.13)	1.51(0.14)	-8.54(0.07)	1.47(0.15)	0.11	0.30(0.33)	0.16(0.17)	-8.28(0.09)	0.69(0.14)	0.74(0.50)	
G140.49+06.07a1	3h37m35.18s	63d07m29.3s	0.14	1.14(0.14)	2.04(0.17)	-16.86(0.07)	1.68(0.16)	0.14	0.40(0.66)	0.42(0.70)	-16.80(0.18)	1.39(0.37)	0.10(0.10)	
G140.77+05.00a1	3h34m26.31s	62d04m47.4s	0.13	0.49(0.16)	0.63(0.14)	-13.46(0.13)	1.21(0.30)	0.10	0.33(0.29)	0.24(0.21)	-13.47(0.09)	0.95(0.16)	0.81(0.53)	
G140.97+05.73a1	3h39m22.25s	62d32m44.1s	0.11	0.66(0.09)	0.58(0.11)	-11.70(0.17)	1.55(0.26)	0.09	0.26(0.88)	0.20(0.68)	-11.76(0.14)	1.02(0.23)	0.10(0.21)	
G142.25+05.43a2	3h46m20.95s	61d31m21.8s	0.05	0.21(0.08)	0.15(0.04)	-10.61(0.08)	0.68(0.20)	
G142.29+07.65a1	3h59m15.72s	63d13m43.0s	0.09	0.67(0.11)	0.79(0.05)	-13.91(0.03)	0.41(1.90)	
G142.29+07.65a2	3h58m43.34s	63d13m58.5s	0.07	1.00(0.13)	1.02(0.08)	-13.74(0.03)	0.96(0.10)	0.07	0.30(0.14)	0.16(0.07)	-13.71(0.05)	0.69(0.06)	0.73(0.26)	
G142.62+07.29a3	3h59m03.10s	62d43m52.5s	0.08	0.25(0.08)	0.33(0.08)	-11.50(0.15)	1.24(0.28)	
G146.49+08.70a1	4h19m34.71s	0.10	0.66(0.23)	0.57(0.11)	-9.56(0.06)	0.81(0.23)	0.07	0.22(0.19)	0.11(0.10)	-9.43(0.08)	0.69(0.06)	0.32(0.23)		
G144.84+00.76a1	3h40m46.62s	56d16m09.1s	0.04	0.13(0.04)	0.19(0.04)	-30.95(0.14)	1.35(0.29)	
G146.11+07.80a1	4h23m37.51s	60d46m46.0s	0.11	0.47(0.15)	0.55(0.11)	-12.26(0.11)	1.08(0.26)	
G146.11+07.80a2	4h23m16.42s	60d44m36.3s	0.09	0.43(0.10)	0.77(0.11)	-11.74(0.12)	1.66(0.30)	0.08	0.25(0.91)	0.24(0.90)	-11.51(0.13)	1.31(0.24)	0.10(0.23)	
G146.11+07.80a3	4h23m18.52s	60d41m25.8s	0.11	0.97(0.19)	0.80(0.10)	-11.75(0.05)	0.77(0.12)	0.08	0.43(0.33)	0.27(0.21)	-11.75(0.06)	0.83(0.12)	0.30(0.18)	
G146.18+08.80b2	4h29m32.32s	61d21m40.1s	0.09	0.49(0.13)	0.58(0.10)	-9.73(0.09)	1.11(0.21)	0.08	0.30(0.40)	0.16(0.21)	-9.73(0.07)	0.69(0.19)	0.18(0.18)	
G146.71-02.05a3	3h56m35.50s	56d04m07.9s	0.06	0.23(0.07)	0.32(0.06)	-1.77(0.13)	1.28(0.29)	
G146.71+02.05b1	3h56m38.72s	56d07m49.2s	0.06	0.44(0.07)	0.51(0.06)	-2.40(0.06)	1.09(0.13)	
G147.01+03.39a1	4h04m38.59s	56d56m09.5s	0.09	2.36(0.21)	1.67(0.08)	-4.74(0.01)	0.67(0.05)	0.09	1.10(0.32)	0.57(0.17)	-4.67(0.03)	0.69(0.01)	0.31(0.07)	
G147.76+09.17a1	4h40m34.18s	60d27m28.7s	0.09	0.73(0.10)	1.08(0.10)	-12.66(0.06)	1.40(0.15)	
G148.00+00.99b1	3h55m18.50s	53d49m00.7s	0.05	0.24(0.09)	0.38(0.08)	-33.61(0.13)	1.50(0.45)	0.05	0.16(0.07)	0.08(0.04)	-33.60(0.09)	0.69(0.12)	0.14(0.05)	
G148.00+00.99b2	3h55m18.50s	53d49m00.7s	0.05	0.14(0.25)	0.12(0.22)	-6.47(0.12)	1.14(0.20)	0.10(0.11)		
G148.00+00.99b2	3h54m56.41s	53d50m23.0s	0.05	0.23(0.08)	0.33(0.07)	-34.36(0.13)	1.32(0.36)	0.04	0.12(0.09)	0.06(0.05)	-34.41(0.07)	0.69(0.15)	0.43(0.27)	
G148.00+00.99b3	3h54m54.37s	53d47m40.9s	0.05	0.54(0.09)	0.56(0.06)	-34.21(0.05)	0.97(0.13)	0.05	0.15(0.15)	0.08(0.08)	-34.13(0.11)	0.69(0.13)	0.87(0.08)	
G148.00+00.99b3	3h54m54.37s	53d47m40.9s	0.05	0.56(0.13)	0.17(0.05)	-6.09(0.09)	0.70(0.32)	
G148.24+00.41a2	3h56m45.85s	53d54m33.4s	0.06	0.30(0.05)	0.67(0.08)	-33.26(0.14)	2.12(0.27)	0.05	0.20(0.33)	0.23(0.38)	-33.43(0.11)	1.52(0.19)	0.10(0.10)	
G149.58+03.45a1	4h18m24.28s	55d12m26.9s	0.09	0.84(0.15)	0.54(0.07)	3.81(0.04)	0.60(0.07)	0.08	0.42(0.65)	0.22(0.34)	3.76(0.05)	0.69(0.03)	0.10(0.10)	
G149.52-01.23a1	3h56m50.88s	51d48m06.9s	0.08	0.65(0.08)	1.68(0.13)	-7.87(0.10)	2.42(0.24)	0.07	0.30(0.85)	0.57(1.63)	-8.24(0.17)	2.55(0.26)	0.10(0.18)	
G150.22+03.91a2	4h23m16.08s	55d04m16.5s	0.08	0.56(0.13)	0.43(0.07)	3.42(0.06)	0.72(0.12)	
G151.08+04.46a1	4h30m30.34s	54d49m28.1s	0.03	0.56(0.09)	0.41(0.03)	2.93(0.02)	0.68(0.10)	0.03	0.19(0.17)	0.10(0.09)	3.07(0.04)	0.72(0.10)	0.23(0.15)	
G153.34+08.00a1	3h48m43.13s	44d07m57.6s	0.09	0.42(0.10)	0.63(0.10)	-1.89(0.11)	1.40(0.26)	0.07	0.21(0.24)	0.13(0.15)	-18.96(0.11)	0.83(0.18)	0.51(0.47)	
G154.07+05.09a1	4h47m19.71s	53d04m33.6s	0.09	0.50(0.12)	0.57(0.09)	3.73(0.09)	1.07(0.20)	0.08	0.27(0.56)	0.29(0.63)	3.91(0.21)	1.43(0.84)	0.10(0.30)	
G154.07+05.21a1	4h48m01.28s	53d09m06.2s	0.09	1.08(0.16)	0.98(0.09)	4.59(0.04)	0.86(0.10)	0.08	0.32(0.26)	0.17(0.14)	4.54(0.06)	0.69(0.06)	0.40(0.27)	
G154.07+05.21a2	4h47m21.78s	53d02m16.2s	0.09	0.62(0.18)	0.72(0.11)	1.08(0.26)	0.08	0.34(0.18)	0.17(0.16)	4.02(0.07)	0.65(0.54)	0.65(0.29)		
G154.90+04.61a1	4h48m30.09s	52d04m25.0s	0.09	1.34(0.16)	0.85(0.08)	2.88(0.03)	0.85(0.09)	0.08	0.41(0.29)	0.34(0.25)	3.29(0.06)	1.11(0.13)	0.82(0.45)	
G154.90+04.61a2	4h48m12.20s	52d09m10.7s	0.09	0.36(0.14)	0.31(0.08)	0.81(0.10)	0.24(0.38)	0.08	0.24(0.38)	0.14(0.23)	3.31(0.10)	0.79(0.28)	0.35(0.42)	

Table 1 — *Continued*

Designation	R.A.	Dec.	HCO ⁺ $J = 1 - 0$						HCN $J = 1 - 0$						
			rms (K)	T_{mb} (K)	$\int T_{\text{mb}} dv$ (K km s ⁻¹)	v_{lsr} (km s ⁻¹)	FWHM (km s ⁻¹)	rms (K)	T_{mb} (K)	$\int T_{\text{mb}} dv$ (K km s ⁻¹)	v_{lsr} (km s ⁻¹)	FWHM (km s ⁻¹)	τ		
G155.67+05.11b2	4h54m03.22s	51d49m09.3s	0.12	0.44(0.16)	0.49(0.12)	4.13(0.15)	1.06(0.30)	
G156.04+06.03a2	5h00m13.70s	52d06m12.5s	0.11	1.61(0.24)	1.12(0.10)	5.80(0.02)	0.65(0.08)	
G156.04+06.03a3	4h59m57.22s	52d05m10.8s	0.09	0.70(0.14)	0.62(0.08)	5.46(0.05)	0.83(0.12)	
G156.20+05.26b1	4h56m59.87s	51d33m28.3s	0.12	0.97(0.19)	0.91(0.11)	5.48(0.05)	0.88(0.14)	
G156.20+05.26b2	4h56m58.21s	51d29m54.7s	0.12	2.35(0.18)	2.24(0.11)	5.52(0.02)	0.89(0.05)	0.10	0.99(0.02)	0.52(0.53)	5.53(0.03)	0.69(0.03)	0.10(0.06)	...	
G157.12-11.56a1	3h51m58.35s	39d03m19.1s	0.12	0.60(0.13)	0.92(0.13)	1.46(0.11)	1.44(0.23)	
G157.12-11.56a2	3h51m55.82s	39d04m12.1s	0.12	0.46(0.12)	0.69(0.13)	1.37(0.14)	1.40(0.27)	
G157.60-12.17a1	3h51m54.01s	38d14m53.8s	0.11	1.06(0.16)	0.85(0.09)	7.56(0.04)	0.76(0.08)	0.11	0.75(0.25)	0.39(0.13)	7.57(0.04)	0.69(0.02)	0.60(0.16)	...	
G157.60-12.17b2	3h51m37.07s	38d11m22.8s	0.10	0.27(0.73)	0.24(0.66)	-1.54(0.22)	1.19(0.55)	0.19(0.38)	...	
G158.24-21.10a2	3h25m06.6s	31d40m06.6s	0.04	0.92(0.04)	0.87(0.04)	7.84(0.02)	0.89(0.05)	0.03	0.63(0.15)	0.35(0.09)	7.92(0.02)	0.75(0.03)	0.10(0.01)	...	
G158.24-21.80a1	3h25m21.37s	30d15m15.3s	0.04	0.22(0.05)	0.28(0.04)	4.16(0.08)	1.22(0.19)	0.03	0.11(0.29)	0.08(0.20)	4.28(0.12)	0.93(0.21)	0.10(0.16)	...	
G158.40-21.86a1	3h25m20.02s	30d15m17.3s	0.03	0.15(0.04)	0.23(0.04)	4.18(0.12)	1.42(0.26)	0.03	0.10(0.08)	0.05(0.04)	4.32(0.08)	0.69(0.07)	0.60(0.40)	...	
G158.40-21.86a2	3h25m38.40s	30d10m36.7s	0.03	0.19(0.04)	0.22(0.03)	4.34(0.09)	1.11(0.18)	0.03	0.09(0.09)	0.05(0.05)	4.60(0.09)	0.69(0.13)	0.68(0.52)	...	
G158.86-21.60a1	3h27m33.95s	30d21m49.2s	0.03	1.86(0.04)	3.12(0.04)	1.58(0.03)	0.03	0.67(0.16)	0.52(0.13)	1.03(0.05)	2.27(0.05)	0.74(0.02)	0.27(0.05)	...	
G158.88-24.18a2	3h25m32.6s	19d53m32.6s	0.03	1.02(0.04)	4.77(0.17)	1.29(0.50)	0.03	0.08(0.19)	0.06(0.13)	-5.17(0.17)	0.89(0.35)	0.10(0.14)	
G159.21-20.12a1	3h33m21.03s	31d06m51.5s	0.11	1.47(0.15)	2.25(0.14)	7.28(0.04)	1.44(0.12)	0.10	0.78(0.33)	0.59(0.26)	6.73(0.04)	1.01(0.08)	0.90(0.35)	...	
G159.23-24.49a1	2h56m10.49s	19d27m00.3s	0.04	0.16(0.05)	0.20(0.04)	4.78(0.13)	1.19(0.31)	0.03	0.07(0.08)	0.08(0.10)	4.17(0.27)	1.62(0.48)	0.30(0.28)	...	
G159.34-24.39a1	3h21m56.63s	27d37m30.8s	0.03	0.06(0.19)	0.07(0.21)	2.59(0.23)	1.43(0.34)	0.10(0.19)	...	
G159.41-34.36a1	2h56m50.29s	19d25m40.4s	0.03	0.17(0.05)	0.15(0.03)	-5.61(0.08)	0.83(0.21)	0.03	0.12(0.17)	0.08(0.12)	-5.16(0.11)	0.93(0.19)	0.10(0.09)	...	
G159.41-34.36a2	2h56m38.45s	19d25m22.0s	0.03	0.17(0.05)	0.18(0.04)	4.99(0.25)	0.98(0.21)	
G159.41-34.36a3	2h56m49.19s	19d25m53.6s	0.04	0.16(0.34)	0.08(0.02)	-5.10(0.07)	0.50(1.06)	0.03	0.06(0.08)	0.03(0.04)	-14.24(0.12)	0.69(0.16)	0.10(0.21)	...	
G159.52+03.26a1	4h59m50.55s	47d39m51.6s	0.12	0.54(0.14)	0.69(0.12)	-15.96(0.11)	1.20(0.23)	0.10	0.20(0.76)	0.29(1.10)	-14.92(0.24)	1.91(0.51)	0.10(0.24)	...	
G159.65-19.68a2	3h35m55.50s	31d14m52.7s	0.03	0.09(0.03)	0.17(0.04)	7.56(0.23)	1.69(0.38)	0.03	0.12(0.17)	0.14(0.20)	7.02(0.11)	1.51(0.39)	0.14(0.14)	...	
G159.65-19.68a3	3h35m40.74s	31d23m59.7s	0.04	0.16(0.05)	0.14(0.03)	6.97(0.09)	0.83(0.18)	0.03	0.09(0.06)	0.05(0.03)	7.07(0.08)	0.74(0.15)	0.85(0.42)	...	
G159.67-34.31a1	2h57m46.41s	19d23m59.1s	0.03	0.09(0.04)	0.23(0.07)	-1.90(0.35)	2.41(0.89)	
G159.76-19.62a1	3h36m46.10s	31d09m39.0s	0.03	0.08(0.10)	0.09(0.12)	8.34(0.13)	1.56(0.40)	0.41(0.44)	...	
G159.76-19.62a2	3h36m31.92s	31d11m36.9s	0.04	0.14(0.07)	0.10(0.03)	8.20(0.09)	0.63(0.25)	
G160.53-09.84a1	4h10m41.45s	38d08m45.9s	0.04	0.33(0.05)	0.59(0.06)	-3.52(0.07)	1.65(0.20)	0.04	0.16(0.30)	0.08(0.16)	-3.59(0.07)	0.69(0.09)	0.10(0.12)	...	
G160.51-17.07a1	3h46m42.68s	32d42m17.0s	0.04	0.13(0.04)	0.24(0.05)	10.19(0.19)	1.80(0.21)	0.04	0.09(0.21)	0.11(0.26)	9.66(0.19)	1.66(0.41)	0.15(0.29)	...	
G160.53-19.72a1	4h10m39.19s	38d06m33.8s	0.04	0.20(0.10)	0.27(0.09)	3.57(0.02)	1.29(0.05)	0.09	0.54(0.66)	0.38(0.07)	3.69(0.07)	0.94(0.14)	0.10(0.08)	...	
G160.62-16.70a1	3h48m17.29s	32d54m55.5s	0.04	0.14(0.04)	0.27(0.05)	9.93(0.19)	1.85(0.35)	0.03	0.18(0.07)	0.14(0.06)	9.73(0.07)	1.05(0.18)	0.10(0.02)	...	
G160.83-09.46a1	4h13m10.09s	38d10m52.4s	0.04	0.16(0.13)	0.09(0.03)	-4.24(0.12)	0.52(0.37)	
G161.21-08.72a2	4h17m02.54s	38d25m28.1s	0.04	0.13(0.06)	0.20(0.04)	-2.45(0.12)	1.20(0.23)	0.03	0.14(0.27)	0.07(0.14)	-3.79(0.06)	0.69(0.08)	0.15(0.21)	...	
G161.34-09.32a1	4h15m19.27s	37d54m32.2s	0.02	0.07(0.02)	0.26(0.05)	-3.79(0.36)	3.36(0.72)	...	0.04	0.12(0.20)	0.06(0.11)	-1.05(0.10)	0.71(0.28)	0.63(0.74)	...
G162.46-08.70a2	4h40m44.48s	37d44m04.1s	0.05	0.16(0.09)	0.12(0.04)	3.56(0.31)	0.69(0.31)	...	0.07	0.30(2.00)	0.20(1.33)	2.51(0.09)	0.88(0.17)	0.10(0.42)	...
G164.94-05.71a2	4h46m56.12s	33d01m21.2s	0.08	0.21(0.45)	0.11(0.23)	2.82(0.10)	0.69(0.15)	0.10(0.13)	...	
G164.92-12.65a3	4h16m13.33s	33d01m40.2s	0.04	0.07(0.17)	0.09(0.23)	4.89(0.28)	1.74(0.71)	0.10(0.15)	...	
G166.99-15.34a1	4h13m44.90s	29d43m37.9s	0.04	0.19(0.08)	0.15(0.04)	4.93(0.09)	0.72(0.24)	0.04	0.07(0.17)	0.09(0.23)	4.89(0.28)	1.74(0.71)	0.10(0.15)	...	
G168.13-16.39a1	4h13m30.36s	28d16m08.7s	0.04	0.16(0.08)	0.09(0.03)	7.16(0.12)	0.54(0.20)	
G168.72-15.48a1	4h18m19.93s	28d24m04.1s	0.05	0.70(0.07)	0.42(0.03)	7.06(0.03)	0.56(0.04)	0.04	0.11(0.06)	0.06(0.03)	7.33(0.07)	0.69(0.03)	0.61(0.28)	...	
G168.72-15.48a2	4h18m32.97s	28d24m41.9s	0.04	0.58(0.07)	0.42(0.03)	7.12(0.03)	0.57(0.06)	0.04	0.16(0.19)	0.08(0.12)	7.17(0.06)	0.69(0.05)	0.17(0.15)	...	
G168.72-15.48a3	4h18m31.77s	28d28m49.1s	0.04	0.36(0.04)	0.49(0.04)	7.38(0.06)	0.29(0.12)	0.03	0.12(0.10)	0.06(0.11)	7.42(0.07)	0.69(1.04)	0.82(0.55)	...	
G169.76-16.15a1	4h19m19.75s	27d14m02.2s	0.04	0.51(0.10)	0.46(0.05)	5.41(0.04)	0.84(0.13)	0.04	0.23(0.24)	0.13(0.14)	5.40(0.06)	0.76(0.13)	0.10(0.07)	...	
G169.98-18.97a1	4h10m51.06s	25d11m10.7s	0.03	0.11(0.04)	0.16(0.04)	1.36(0.30)	1.36(0.18)	0.03	0.09(0.12)	0.06(0.08)	6.33(0.09)	0.83(0.13)	1.67(1.54)	...	
G170.00-16.14a1	4h19m56.87s	27d06m34.3s	0.05	0.26(0.11)	0.37(0.08)	6.48(0.14)	1.33(0.49)	0.05	0.16(1.01)	0.08(0.53)	6.76(0.09)	0.69(0.36)	0.13(0.56)	...	
G170.13-16.06a2	4h20m50.43s	27d03m08.9s	0.05	0.27(0.09)	0.16(0.04)	7.08(0.08)	0.54(0.12)	0.03	0.12(0.10)	0.06(0.11)	7.42(0.07)	0.69(1.04)	0.82(0.55)	...	
G170.13-16.06a2	4h20m44.25s	27d02m32.4s	0.06	0.20(0.06)	0.29(0.06)	6.43(0.14)	1.36(0.31)	0.03	0.10(0.12)	0.06(0.08)	6.33(0.09)	0.83(0.13)	1.67(1.54)	...	
G170.99-15.81a1	4h24m05.27s	26d35m34.9s	0.03	0.10(0.06)	0.06(0.29)	0.22(0.31)	-2.90(0.13)	1.39(0.22)	0.10(0.08)	...
G171.34+02.59a1	5h34m31.47s	37d38m40.0s	0.06	0.37(0.06)	0.81(0.09)	-2.59(0.11)	2.03(0.27)	0.06	0.21(0.29)	0.22(0.31)	0.22(0.31)	
G171.34+02.59b1	5h34m06.55s	37d58m37.4s	0.10	0.64(0.11)	0.70(0.11)	1.43(0.12)	0.59(0.11)	0.06	0.31(0.07)	0.23(0.07)	1.93(0.12)	1.81(0.13)	0.10(0.08)	...	
G171.34+02.59b2	5h34m06.65s	37d33m26.2s	0.06	0.31(0.07)	0.63(0.07)	1.32(0.12)	0.59(0.11)	0.06	0.31(0.07)	0.23(0.07)	1.93(0.12)	1.81(0.13)	0.10(0.08)	...	
G171.34+02.59b3	5h34m07.00s	38d37m17.2s	0.07	0.23(0.06)	0.23(0.06)	0.50(0.11)	0.50(0.11)	0.07	0.23(0.06)	0.23(0.06)	0.50(0.11)	0.50(0.11)	0.10(0.07)	...	

Table 1 — *Continued*

Designation	R.A.	Dec.	HCO ⁺ $J = 1 - 0$						HCN $J = 1 - 0$					
			rms (K)	T_{mb} (K)	$\int T_{\text{mb}} dv$ (K km s ⁻¹)	v_{lsr} (km s ⁻¹)	FWHM (km s ⁻¹)	rms (K)	T_{mb} (K)	$\int T_{\text{mb}} dv$ (K km s ⁻¹)	v_{lsr} (km s ⁻¹)	FWHM (km s ⁻¹)	τ	
G171.84-05.22a1	5h04m04.47s	32d43m44.7s	0.05	0.320(0.13)	0.200(0.04)	7.15(0.05)	0.59(0.21)
G171.80-15.32a1	4h27m55.82s	26d19m29.8s	0.04	0.360(0.11)	0.230(0.03)	6.91(0.04)	0.58(0.16)
G171.91-15.65a1	4h27m04.11s	26d06m37.3s	0.05	0.53(0.10)	0.27(0.04)	6.65(0.06)	0.47(0.06)
G172.06-15.2a2	4h29m11.9s	0.04	0.27(0.07)	0.23(0.04)	6.65(0.07)	0.83(0.16)	0.04	0.11(0.19)	0.06(0.11)	6.52(0.09)	0.69(0.50)	0.21(0.27)	...	
G172.15-16.02a1	4h26m59.52s	25d37m13.4s	0.04	0.16(0.07)	0.10(0.03)	9.45(0.07)	0.55(0.50)
G172.15-16.02a2	4h26m46.31s	25d39m59.3s	0.04	0.74(10.16)	0.320(0.05)	6.57(0.02)	0.41(5.63)
G172.57-18.11a1	4h21m06.04s	23d55m59.5s	0.04	0.14(0.09)	0.11(0.04)	3.44(0.17)	0.72(0.37)
G172.85-02.27a1	5h36m53.79s	36d10m32.8s	0.13	3.68(0.23)	10.65(0.47)	-17.57(0.03)	2.72(0.12)	0.12	1.09(0.25)	1.74(0.41)	-17.80(0.05)	2.13(0.09)	0.10(0.01)	...
G172.85-14.74a2	4h33m16.68s	25d54m07.2s	0.03	0.10(0.15)	0.05(0.10)	12.18(0.10)	0.70(0.70)	0.10(0.10)
G172.94-05.49a1	5h06m15.85s	31d43m43.0s	0.09	0.51(0.16)	0.41(0.08)	7.12(0.08)	0.75(0.19)
G172.92-16.74b1	4h26m40.91s	24d41m50.3s	0.04	0.51(0.45)	0.22(0.03)	6.45(0.02)	0.41(0.36)	0.03	0.13(0.11)	0.07(0.06)	6.57(0.07)	0.69(0.02)	0.36(0.23)	...
G173.10+07.23a1	5h58m57.87s	38d32m01.9s	0.07	0.57(0.11)	0.62(0.08)	0.32(0.06)	1.01(0.15)	0.07	0.22(0.22)	0.12(0.13)	0.53(0.09)	0.75(0.19)	0.19(0.13)	...
G173.12-13.32a1	4h38m32.16s	26d44m02.1s	0.04	0.10(0.40)	0.05(0.21)	5.32(0.11)	0.69(0.11)	0.10(0.25)
G173.36-16.27a1	4h23m21.53s	0.04	0.42(0.16)	0.22(0.03)	7.03(0.04)	0.48(0.17)
G173.60-17.89a1	4h24m47.55s	23d21m08.8s	0.09	0.28(0.09)	0.49(0.11)	4.36(0.19)	1.63(0.39)
G173.89-17.64a2	4h26m17.12s	23d20m54.5s	0.05	0.29(17.98)	0.13(0.10)	5.40(0.05)	0.41(25.42)
G173.95-13.74a1	4h39m28.05s	25d48m13.9s	0.05	0.99(0.08)	0.65(0.04)	6.60(0.02)	0.61(0.03)	0.04	0.32(0.09)	0.16(0.05)	6.54(0.03)	0.69(0.01)	0.10(0.01)	...
G174.06-15.8 a1	4h32m31.08s	24d23m25.3s	0.05	1.47(0.07)	1.67(0.05)	6.11(0.02)	1.07(0.04)	0.05	0.40(0.14)	0.21(0.07)	6.08(0.03)	0.69(0.02)	0.46(0.14)	...
G174.44-15.75a1	4h33m56.07s	24d10m21.0s	0.05	1.31(0.08)	0.94(0.04)	6.76(0.01)	0.67(0.03)	0.04	0.43(0.14)	0.25(0.22)	6.76(0.04)	0.78(0.04)	0.14(0.08)	...
G174.70-15.48a1	4h35m38.97s	24d07m34.5s	0.11	3.61(0.19)	2.80(0.09)	5.89(0.01)	0.73(0.03)	0.10	0.97(0.71)	0.50(0.37)	5.92(0.03)	0.69(0.04)	0.15(0.08)	...
G175.16-16.74a2	4h32m26.15s	22d57m46.0s	0.04	0.12(0.06)	0.09(0.03)	5.81(0.16)	0.71(0.23)
G175.49-16.89a2	4h33m28.95s	22d41m01.2s	0.03	0.10(0.04)	0.26(0.06)	5.89(0.31)	0.41(0.67)
G176.97-20.38a1	4h22m59.96s	20d01m57.0s	0.09	0.41(1.12)	0.18(0.05)	7.38(0.06)	0.41(1.11)
G176.94-04.63a1	5h57m00.65s	33d56m44.5s	0.04	0.13(0.08)	0.13(0.05)	-17.48(0.16)	0.96(0.49)
G177.14-01.21a1	5h33m53.60s	30d42m47.9s	0.04	0.09(0.17)	0.05(0.11)	-16.89(0.14)	0.69(0.13)	0.10(0.12)	...	
G177.62-20.36a1	4h27m17.68s	18d52m29.1s	0.04	0.51(1.78)	0.22(0.03)	7.89(0.02)	0.41(1.43)
G178.28-00.61a2	5h39m06.75s	30d04m48.9s	0.05	0.16(0.07)	0.25(0.06)	-1.51(0.16)	1.50(0.56)
G180.92+04.53a1	6h05m46.75s	6d24m11.4s	0.12	0.56(0.17)	0.90(0.16)	1.87(0.12)	1.51(0.37)	0.11	0.34(0.27)	0.18(0.43)	1.71(0.12)	0.72(1.56)	3.00(1.50)	...
G181.16+04.33a1	6h05m37.15s	30d02m00.75s	0.07	0.80(0.16)	0.77(0.09)	0.53(0.05)	0.91(0.15)	0.06	0.37(0.92)	0.25(0.62)	0.48(0.07)	0.89(0.12)	0.10(0.16)	...
G181.16+04.33a2	6h05m27.15s	30d06m33.7s	0.08	0.45(0.09)	0.82(0.10)	1.24(0.10)	1.24(0.10)	0.07	0.31(0.12)	0.16(0.07)	1.39(0.04)	0.69(0.09)	1.05(0.32)	...
G181.42-03.73a1	5h34m39.21s	25d42m26.5s	0.08	1.01(0.12)	1.26(0.09)	-5.47(0.04)	1.18(0.11)	0.06	0.33(0.62)	0.29(0.54)	5.49(0.08)	1.15(0.24)	0.13(0.16)	...
G181.71-04.16a1	6h06m07.84s	29d34m43.0s	0.12	0.75(0.20)	0.55(0.10)	3.42(0.06)	0.69(0.14)
G181.84+00.31a1	5h51m41.43s	2/d35m38.5s	0.09	0.28(2.11)	0.14(1.10)	2.17(0.27)	0.69(0.27)	0.10(0.48)	...	
G181.84+00.31a2	5h51m22.63s	27d29m38.5s	0.10	1.77(0.16)	1.80(0.10)	1.96(0.02)	0.95(0.07)	0.08	1.10(0.68)	0.62(0.39)	1.95(0.02)	0.75(0.06)	0.10(0.04)	...
G181.84+00.31b1	5h51m18.63s	27d28m08.5s	0.09	0.81(0.15)	0.69(0.08)	1.90(0.05)	0.80(0.11)	0.09	0.43(0.68)	0.27(0.44)	2.06(0.09)	0.85(0.27)	0.18(0.21)	...
G181.84+00.31b2	5h51m26.63s	27d29m08.5s	0.13	1.69(0.16)	2.45(0.14)	2.30(0.04)	1.36(0.10)	0.11	0.90(0.46)	0.80(0.42)	2.16(0.05)	1.18(0.11)	0.10(0.03)	...
G182.29-02.27a1	5h49m12.0s	0.09	0.50(0.12)	0.59(0.09)	0.82(0.08)	1.01(0.12)	0.80(0.20)	0.08	0.55(0.70)	0.34(0.44)	2.62(0.05)	0.83(0.13)	0.15(0.13)	...
G185.80-09.12a1	5h25m18.01s	19d10m08.1s	0.09	1.54(0.13)	1.83(0.10)	-2.59(0.03)	1.12(0.07)	0.08	0.55(0.70)	0.34(0.44)	2.62(0.05)	0.83(0.13)	0.15(0.13)	...
G185.80-09.12a2	5h25m13.68s	19d15m17.1s	0.10	0.48(0.15)	0.65(0.12)	-2.05(0.10)	1.28(0.32)
G190.08-13.51a2	5h19m30.38s	13d14m41.3s	0.12	0.43(0.12)	0.60(0.12)	1.18(0.14)	1.31(0.27)	0.09	0.22(0.43)	0.16(0.31)	6.19(0.15)	0.95(0.23)	0.10(0.12)	...
G190.08-08-13.54a4	5h18m27.24s	12d10m15.3s	0.06	0.32(0.46)	0.17(0.04)	1.08(0.09)	0.51(0.73)	0.05	0.13(0.44)	0.08(0.29)	0.77(0.17)	0.86(0.48)	0.50(1.24)	...
G190.17-17-13.78a1	5h18m52.73s	13d02m16.3s	0.03	0.10(0.05)	0.24(0.06)	0.68(0.26)	0.27(0.86)	0.04	0.13(0.16)	0.07(0.09)	0.37(0.09)	0.69(0.39)	0.18(0.17)	...
G190.15-14.34a1	5h16m53.96s	12d45m17.6s	0.07	0.33(0.06)	0.57(0.08)	1.53(0.11)	1.60(0.22)	0.07	0.20(0.13)	1.46(0.16)	1.76(0.33)	0.10(0.04)
G190.15-14.34a2	5h16m44.63s	12d45m13.6s	0.09	0.44(0.11)	0.68(0.11)	1.55(0.13)	1.44(0.28)	0.08	0.53(0.53)	0.38(0.39)	1.46(0.05)	0.96(0.14)	0.19(0.14)	...
G190.15-14.34a3	5h16m23.16s	12d45m39.6s	0.10	0.33(0.17)	0.31(0.10)	1.78(0.14)	0.88(0.37)	0.09	0.29(0.28)	0.20(0.19)	1.40(0.08)	0.91(0.16)	0.81(0.59)	...
G191.03-16.74a1	5h10m17.90s	10d46m15.7s	0.10	0.51(0.15)	0.34(0.07)	2.19(0.07)	0.63(0.14)	0.07	0.22(0.19)	0.17(0.15)	1.82(0.10)	1.00(0.21)	0.35(0.22)	...
G191.51-00.76a2	6h08m00.90s	18d36m14.7s	0.03	0.09(0.05)	0.14(0.05)	-0.10(0.25)	1.50(0.61)
G192.12-10.90a1	5h32m53.23s	12d56m15.6s	0.10	0.62(0.11)	0.69(0.09)	10.02(0.08)	1.04(0.13)	0.09	0.38(0.51)	0.26(0.35)	9.95(0.08)	0.90(0.23)	0.23(0.24)	...
G192.12-10.90a2	5h32m41.70s	12d55m15.6s	0.09	0.72(0.11)	1.20(0.11)	9.63(0.08)	1.58(0.18)	0.08	0.37(0.37)	0.46(0.46)	9.84(0.10)	1.66(0.17)	0.10(0.06)	...
G192.12-10.90a3	5h32m34.10s	12d51m30.6s	0.09	0.39(0.07)	1.15(0.14)	9.99(0.17)	2.77(0.34)
G192.28-28-13.33a1	5h31m39.36s	12d31m49.8s	0.08	1.28(0.09)	2.17(0.10)	10.10(0.04)	1.59(0.09)	0.09	0.72(0.49)	0.60(0.41)	10.19(0.04)	1.10(0.12)	0.21(0.11)	...
G192.28-28-13.33a2	5h31m32.43s	12d31m20.8s	0.09	0.61(0.09)	1.25(0.12)	10.28(0.09)	1.94(0.22)	0.08	0.77(0.15)	0.42(0.08)	10.21(0.03)	0.72(0.01)	0.16(0.02)	...
G192.28-28-13.33a3	5h31m42.89s	12d33m39.8s	0.09	0.98(0.10)	1.53(0.10)	10.05(0.05)	1.47(0.12)	0.08	0.36(0.37)	0.31(0.32)	10.16(0.08)	1.14(0.19)	0.25(0.20)	...

Table 1 — Continued

Designation	R.A.	Dec.	HCO ⁺ $J = 1 - 0$										HCN $J = 1 - 0$				
			rms (K)	T_{mb} (K)	$\int T_{\text{mb}} d\nu$ (K km s ⁻¹)	ν_{lsr} (km s ⁻¹)	FWHM (km s ⁻¹)	rms (K)	T_{mb} (K)	$\int T_{\text{mb}} d\nu$ (K km s ⁻¹)	ν_{lsr} (km s ⁻¹)	FWHM (km s ⁻¹)	τ				
G192.32-11.87al	5h29m41.06s	12d21m07.5s	0.04	0.24(0.05)	0.32(0.04)	11.78(0.08)	1.27(0.20)	0.03	0.12(0.04)	0.12(0.05)	11.83(0.10)	1.31(0.27)	0.11(0.01)				
G192.54-11.56al	5h31m26.82s	12d10m33.4s	0.10	0.80(0.20)	0.71(0.10)	10.57(0.05)	0.83(0.17)	0.09	0.40(0.69)	0.30(0.52)	10.36(0.08)	0.99(0.13)	0.10(0.11)				
G194.80-03.41al	6h04m56.24s	14d31m13.0s	0.15	1.18(0.13)	3.19(0.22)	12.67(0.09)	2.54(0.22)	0.13	0.58(0.21)	0.90(0.35)	12.70(0.12)	2.06(0.29)	0.10(0.02)				
G195.09-16.4 al	5h17m47.74s	7d24m58.1s	0.09	0.46(0.13)	0.46(0.10)	-2.07(0.12)	1.15(0.25)	0.10	0.34(0.46)	0.33(0.45)	-0.87(0.12)	1.30(0.25)	0.19(0.19)			
G195.00-16.95al	5h19m55.82s	7d39m03.2s	0.10	0.77(0.14)	0.85(0.10)	1.05(0.14)	0.85(0.08)	0.10	0.55(0.29)	0.85(0.29)	1.05(0.14)	1.30(0.25)	0.19(0.19)				
G195.00-16.95s2	5h19m50.42s	7d34m57.2s	0.10	0.52(0.22)	0.47(0.11)	1.27(0.41)	0.77	0.20(0.29)	0.30(0.45)	0.84(0.21)	2.02(0.45)	0.10(0.14)					
G196.21-15.50al	5h25m12.02s	7d10m16.9s	0.08	0.27(0.11)	0.37(0.09)	3.70(0.15)	1.27(0.41)	0.07	0.20(0.29)	0.30(0.45)	0.84(0.21)	2.02(0.45)	0.10(0.14)				
G198.03-15.24al	5h29m33.47s	5d52m03.2s	0.07	0.27(0.10)	0.36(0.08)	-0.13(0.13)	1.26(0.35)	0.04	0.13(0.11)	0.07(0.06)	-0.15(0.08)	0.69(0.16)	1.61(0.04)				
G198.03-15.24a2	5h29m45.60s	5d45m21.2s	0.06	0.36(0.15)	0.24(0.05)	0.26(0.06)	1.63(0.23)	0.06	0.18(0.16)	0.13(0.14)	0.12(0.22)	0.92(0.56)	0.10(0.09)				
G198.56-09.10al	5h52m24.65s	8d22m07.0s	0.10	1.17(0.11)	1.85(0.12)	11.90(0.05)	1.49(0.11)	0.09	0.47(0.32)	0.38(0.27)	11.75(0.07)	1.08(0.15)	0.27(0.14)				
G199.88+00.93a1	6h30m45.17s	12d01m53.0s	0.10	0.66(0.14)	0.64(0.09)	6.50(0.07)	0.91(0.14)	0.09	0.33(0.24)	0.17(0.13)	0.46(0.07)	0.70(0.10)	0.59(0.34)				
G200.34-10.97al	5h49m09.60s	5d59m51.0s	0.07	0.32(0.10)	0.50(0.09)	13.72(0.13)	1.48(0.38)	0.09	0.21(0.40)	0.21(0.40)	0.37(0.11)	0.77(0.11)	0.11(0.14)			
G200.34-10.97a2	5h49m05.33s	5d55m30.0s	0.08	0.79(0.11)	0.96(0.09)	13.48(0.05)	1.13(0.12)	0.07	0.37(0.69)	0.21(0.40)	0.37(0.06)	13.42(0.06)	0.79(0.40)	0.35(0.61)			
G200.34-10.97a3	5h49m09.67s	5d55m07.0s	0.10	0.75(0.12)	0.79(0.11)	13.84(0.06)	0.98(0.20)	0.08	0.26(0.58)	0.16(0.35)	0.26(0.58)	1.37(0.08)	1.73(0.08)	1.16(0.12)	0.10(0.15)		
G201.13-00.31b1	6h30m53.51s	10d38m40.9s	0.10	1.54(0.12)	2.11(0.11)	5.21(0.03)	1.29(0.08)	0.09	0.66(1.60)	0.58(1.40)	0.58(1.40)	5.28(0.05)	1.16(0.12)	0.10(0.15)			
G201.26+00.46b2	6h31m29.50s	10d38m18.6s	0.09	0.21(0.85)	0.14(0.57)	0.17(0.13)	0.89(0.24)	1.51(0.13)	0.89(0.24)	0.10(0.25)		
G201.44+00.65a2	6h32m24.91s	10d25m07.7s	0.07	0.36(0.06)	1.30(0.13)	4.79(0.16)	3.35(0.39)	0.09	0.37(0.69)	0.21(0.40)	0.37(0.11)	0.77(0.11)	0.11(0.14)			
G201.59+00.55a1	6h32m26.05s	10d24m51.5s	0.12	0.39(0.08)	1.37(0.20)	4.72(0.25)	3.28(0.48)	0.10	0.20(1.36)	0.28(1.86)	0.85(0.24)	1.82(0.42)	0.10(0.42)			
G202.21-09.17a2	5h59m04.44s	5d12m04.48s	0.10	0.20(1.36)	0.28(1.86)	0.85(0.24)	1.82(0.42)	0.10(0.42)				
G202.30-08.9al	6h00m10.81s	5d14m40.2s	0.11	0.36(0.11)	0.96(0.18)	12.05(0.27)	2.49(0.61)	0.09	0.30(0.85)	0.28(0.79)	10.30(0.17)	1.22(0.52)	0.41(0.92)			
G202.30-08.91b2	6h00m15.81s	5d15m46.2s	0.07	0.47(0.17)	0.40(0.08)	12.62(0.08)	0.80(0.25)	0.08	0.17(0.14)	0.09(0.07)	12.36(0.07)	0.69(0.08)	1.81(1.05)			
G202.30-08.91b3	6h00m11.21s	5d14m53.2s	0.09	0.66(0.11)	0.74(0.09)	12.26(0.06)	1.05(0.13)	0.09	0.30(0.85)	0.28(0.79)	10.30(0.17)	1.22(0.52)	0.41(0.92)				
G203.20-11.24a1	5h53m44.67s	3d22m41.8s	0.11	0.75(0.23)	0.39(0.08)	9.68(0.08)	1.49(0.11)	0.09	0.30(0.85)	0.28(0.79)	10.30(0.17)	1.22(0.52)	0.41(0.92)				
G203.75-08.49a1	6h04m30.25s	4d12m02.1s	0.12	0.36(0.09)	0.66(0.12)	11.55(0.16)	1.69(0.30)	0.09	0.14(0.51)	0.07(0.27)	1.54(0.08)	0.69(0.32)	0.10(0.24)			
G204.49-11.33a1	5h55m51.49s	2d16m03.0s	0.03	0.10(0.05)	0.16(0.05)	1.55(0.24)	1.52(0.61)	0.04	0.14(0.51)	0.07(0.27)	1.54(0.08)	0.69(0.32)	0.10(0.24)				
G204.49-11.33a2	5h55m37.07s	2d11m01.3s	0.03	0.11(0.04)	0.19(0.05)	1.36(0.22)	1.57(0.42)	0.09	0.37(0.67)	0.52(0.95)	8.66(0.12)	1.87(0.22)	0.10(0.11)			
G204.82-13.88a1	5h47m22.56s	0d41m05.8s	0.10	0.48(0.07)	1.58(0.16)	8.47(0.16)	3.08(0.33)	0.09	0.43(0.38)	0.48(0.43)	9.39(0.12)	1.48(0.22)	0.31(0.21)				
G626.87-04.36a1	6h24m43.71s	3d22m14.4s	0.14	0.70(0.33)	0.54(0.03)	11.13(0.03)	1.54(0.03)	0.57(0.21)				
G207.35-19.82a1	5h30m45.49s	4d10m59.2s	0.12	2.02(0.15)	3.32(0.15)	6.91(0.14)	11.71(0.01)	0.10	1.33(0.03)	1.33(0.03)	1.33(0.03)	1.11(0.10)	0.57(0.21)				
G207.35-19.82a2	5h31m03.43s	-9d33m06.88	0.12	4.89(0.15)	6.91(0.14)	11.71(0.01)	1.33(0.05)	0.10	2.33(0.20)	2.48(0.22)	11.57(0.02)	1.41(0.03)	0.10(0.00)				
G215.41-16.39a1	5h56m58.14s	-9d06m07.6s	0.08	0.70(0.13)	0.63(0.07)	1.03(0.12)	0.84(0.12)	0.07	0.42(0.49)	0.22(0.26)	11.33(0.06)	0.69(0.07)	0.10(0.10)				
G215.70-15.05a1	5h53m36.31s	-10d24m45.6s	0.10	0.58(0.10)	0.76(0.10)	8.76(0.10)	9.17(0.09)	0.11	1.22(0.15)	0.39(0.64)	11.91(0.11)	1.33(0.21)	0.10(0.10)				
G215.88-17.58a1	6h13m58.16s	-9d21m42.4s	0.15	1.74(0.31)	1.26(0.13)	11.80(0.03)	0.68(0.10)	0.13	0.84(0.88)	0.44(0.46)	11.62(0.04)	0.69(0.07)	0.13(0.09)				
G217.13-12.54a1	6h09m56.56s	-10d11m59.0s	0.14	0.67(0.20)	1.11(0.19)	9.46(0.13)	1.56(0.38)	0.13	0.35(0.55)	0.20(0.33)	9.57(0.13)	0.78(0.28)	0.10(0.10)				
G217.70-16.12a1	6h01m51.49s	-11d23m51.0s	0.12	0.29(0.75)	0.33(0.86)	4.78(0.21)	1.52(0.35)	0.10(0.16)				
G224.47-00.65a1	7h10m00.00s	-10d29m30.4s	0.14	0.54(0.21)	0.72(0.17)	13.75(0.14)	1.26(0.39)	0.13	0.27(0.46)	0.19(0.33)	13.83(0.16)	0.93(0.25)	0.10(0.10)				
G226.29-00.63a1	7h14m18.37s	-12d16m11.0s	0.15	1.96(0.15)	5.14(0.24)	14.84(0.06)	2.46(0.15)	0.16	1.70(0.20)	2.60(0.32)	14.99(0.04)	2.03(0.07)	0.10(0.01)				
G226.36-00.50a1	7h14m18.27s	-12d16m21.0s	0.18	1.34(0.12)	4.08(0.25)	14.89(0.09)	2.85(0.20)	0.11	0.11(0.04)	0.11(0.04)	0.11(0.04)	0.11(0.04)	0.11(0.04)			

Table 2

Derived Parameters

Designation	R_{gal} (kpc)	$\tau_{13\text{CO}}$	$\tau_{\text{C}^{18}\text{O}}$	$T_{\text{ex}}^{\text{CO}}$ (K)	$N_{13\text{CO}}^{\text{ex}}$ (10^{15} cm ⁻²)	$N_{\text{C}^{18}\text{O}}^{\text{ex}}$ (10^{15} cm ⁻²)	$N_{\text{HCN}}^{\text{ex}}$ (10^{12} cm ⁻²)	N_{H_2} (10^{21} cm ⁻²)	$N_{\text{HCN}}^{\text{+}}$ (10^{-11})	X_{HCN} (10^{-11})	
G026.45+08.02a1	8.10	0.45	1.79	0.40	0.58	11.01(0.56)	14.71(1.23)	1.81(0.31)	0.74(0.14)	0.62(0.92)	10.37(1.79)
G031.26-05.37a1	8.61	14.67	0.82	0.35	11.70(0.55)	6.90(0.52)	0.58(0.21)	0.46(0.17)	0.46(0.17)	5.39(0.41)	8.50(3.28)
G038.36-00.95a1	7.60	1.20	1.32	0.16	10.73(0.31)	21.45(0.95)	2.50(0.29)	0.52(0.12)	0.12(0.48)	4.11(0.06)	1.52(0.35)
G043.02+08.36a1	8.39	0.15	0.57	0.32	11.66(0.57)	4.19(0.34)	0.29(0.13)	1.14(0.37)	0.11(0.04)	3.13(0.26)	36.32(12.21)
G057.17-03.41a1	8.11	0.77	0.13	0.10	12.00(0.33)	11.20(0.55)	1.45(0.25)	0.11(0.04)	0.11(0.04)	8.34(0.43)	1.27(0.48)

Table 2 — *Continued*

Designation	R_{gal} (kpc)	Dist kpc	$\tau_{13\text{CO}}$	$\tau_{\text{C}^{18}\text{O}}$	τ_{HCO^+}	$T_{\text{ex}}^{\text{CO}}$ (K)	$N_{13\text{CO}}$ (10^{15} cm^{-2})	$N_{\text{C}^{18}\text{O}}$ (10^{15} cm^{-2})	N_{HCO^+} (10^{12} cm^{-2})	N_{HCN} (10^{12} cm^{-2})	N_{HCO^+} (10^{21} cm^{-2})	X_{HCN} (10^{-11})	
G058.97-01.66b1	7.63	2.10	0.26	0.18	9.67(0.59)	3.77(0.60)	... 38.37(0.32)	2.77(0.32)	0.16(0.05)	2.41(0.38)	6.49(2.49)	...	
G070.44-01.54a2	8.17	1.25	0.73	0.07	0.42	16.04(0.17)	48.86(3.07)	7.35(1.38)	4.05(0.82)	1.43(3.60)	16.13(1.86)	25.09(5.85)	8.88(22.36)
G070.72-00.63a1	8.04	2.26	0.57	0.12	0.08	14.72(0.50)	56.63(1.23)	0.57(0.14)	0.57(0.04)	41.57(7.81)	1.37(0.42)
G074.11+00.11a1	8.25	3.45	0.87	0.16	0.12	12.59(0.15)	43.38(0.87)	5.95(1.01)	0.11(0.04)	35.43(6.02)	0.30(0.11)
G084.79-01.11a1	8.59	2.22	0.72	0.13	1.57	15.36(0.27)	42.31(1.50)	3.71(0.57)	8.17(1.48)	4.15(1.41)	23.96(3.69)	34.08(8.09)	17.34(6.48)
G084.79-01.11a2	8.59	2.22	1.13	0.29	0.21	15.40(0.20)	56.63(1.23)	8.68(0.40)	1.42(0.28)	5.16(2.61)	2.53(0.51)	9.22(9.47)	...
G084.79-01.11a3	8.59	2.22	0.91	0.18	0.10	14.05(0.19)	41.88(1.40)	5.51(0.36)	0.50(0.11)	1.30(3.73)	35.56(2.30)	1.40(0.32)	3.65(10.49)
G084.79-01.11a4	8.49	0.10	0.98	0.23	0.31	13.40(0.23)	43.24(1.59)	4.20(0.38)	0.62(0.13)	2.30(2.17)	26.50(2.41)	2.33(0.53)	8.67(8.22)
G089.75-02.16b1	8.52	0.62	0.34	0.10	...	14.78(0.18)	8.37(0.30)	0.23(0.07)	...	0.77(1.18)	1.45(0.46)	...	53.13(82.91)
G089.93-01.94a1	8.55	0.95	0.72	0.25	0.25	14.14(0.57)	8.20(0.54)	0.57(0.16)	...	6.34(0.42)	8.95(2.66)
G093.12-10.40a2	8.52	0.24	0.75	0.09	...	12.59(0.21)	8.04(0.29)	0.34(0.10)	...	2.14(0.61)	13.40(31.16)
G093.44-04.66a1	0.56	0.39(0.94)
G093.44-04.66a2	8.51	0.12	0.80	0.17	0.71	11.22(0.23)	12.74(0.45)	1.85(0.20)	1.50(0.30)	1.45(1.16)	11.71(1.25)	12.81(2.92)	12.39(9.98)
G093.62-04.44a1	...	0.73	...	0.55	1.36(0.28)	1.31(0.79)
G093.75-04.59a1	...	1.17	...	0.30	0.65(0.20)	0.88(6.53)
G093.91+10.02a2	8.71	1.40	2.31	0.27	0.12	7.95(0.78)	12.92(1.82)	1.34(0.30)	0.11(0.04)	...	8.88(2.00)	1.20(0.49)	...
G096.37+0.29a1	8.76	1.38	1.53	0.09	0.97	8.97(0.41)	10.45(0.78)	...	0.08(0.03)	...	8.42(0.63)	0.89(0.40)	...
G097.09+0.12a1	8.75	1.27	1.18	0.09	0.16	8.56(0.20)	8.32(0.41)	0.52(0.16)	0.14(0.04)	...	3.50(0.07)	3.99(1.67)	...
G097.77+08.59a2	0.86	...	0.08	0.15(0.05)
G098.50-03.24a1	8.87	1.59	0.71	0.10	0.25	11.59(0.21)	8.10(0.28)	0.75(0.11)	0.78(0.24)	0.79(0.51)	5.16(0.79)	15.08(1.18)	15.33(10.09)
G098.96+13.68a1	8.76	1.17	1.02	0.14	0.17	9.92(0.38)	7.43(0.47)	0.52(0.15)	0.26(0.07)	3.51(1.01)	7.55(2.88)
G102.34+15.96a2	2.17	...	0.13	0.14(0.04)	0.30(0.52)
G102.72+15.36a1	8.58	0.32	0.81	...	0.12	9.38(0.47)	14.47(1.23)	...	0.27(0.08)	11.23(0.95)	2.45(0.73)
G102.72+15.36a2	0.78	...	0.07	0.13(0.05)
G102.72-25.98a1	0.47	...	0.08	0.07(0.03)
G103.22-15.23a1	8.56	0.24	0.62	0.19	0.08	12.12(0.30)	8.31(0.39)	0.31(0.09)	0.07(0.05)	...	2.00(0.55)	3.74(2.55)	...
G103.90+0.39a1	...	1.11	...	0.08	0.13(0.05)
G104.78+11.49a1	9.07	1.66	0.61	0.08	0.34	12.31(0.24)	9.61(0.32)	1.21(0.17)	0.44(0.09)	0.40(0.42)	8.72(1.22)	5.04(1.28)	4.64(4.82)
G105.55+0.40a1	8.78	0.90	0.70	0.09	0.20	14.97(0.35)	11.60(0.51)	1.01(0.25)	0.55(0.11)	0.65(4.96)	6.84(1.69)	8.12(2.58)	9.46(72.62)
G106.30+13.57a1	9.11	1.66	0.83	0.21	1.21	12.48(0.30)	13.57(0.60)	2.17(0.26)	0.47(0.47)	...	15.80(1.86)	2.96(3.03)	...
G108.85-00.80a1	8.56	0.18	0.61	0.10	0.66	15.84(0.17)	30.68(0.66)	3.87(0.35)	4.73(0.98)	2.41(4.20)	24.80(2.23)	19.07(4.30)	9.70(16.94)
G108.85-00.80a2	8.56	0.18	0.69	0.11	0.32	16.64(0.17)	32.87(0.61)	3.36(0.30)	15.59(3.03)	3.89(2.63)	21.56(1.92)	72.32(15.44)	18.06(12.28)
G110.65+09.65a1	8.61	0.30	1.41	0.25	0.29	11.55(0.12)	22.35(0.43)	2.30(0.53)	0.87(0.17)	0.99(0.86)	14.92(3.42)	5.86(1.76)	6.65(5.94)
G111.33+19.94a2	9.02	1.22	1.34	0.29	0.09	9.34(0.32)	9.75(0.57)	0.98(0.17)	0.32(0.08)	...	7.02(1.20)	4.50(1.40)	...
G111.66+20.20a1	9.06	1.30	1.40	0.17	1.17	11.34(0.44)	15.95(0.90)	1.28(0.19)	0.65(0.13)	0.78(1.24)	9.21(1.38)	7.08(1.78)	8.48(13.55)
G111.77+20.26a1	9.07	1.31	0.88	0.14	0.23	13.43(0.69)	14.22(1.04)	0.91(0.22)	0.84(0.16)	0.88(1.15)	6.58(1.60)	12.69(3.95)	13.33(17.73)
G112.60+08.53a2	8.85	0.83	0.56	...	0.05	12.32(0.33)	11.05(0.55)	...	0.21(0.06)	...	9.07(0.45)	2.27(0.64)	...
G113.42+16.97a1	8.94	0.99	0.69	0.05	0.05	10.54(0.17)	11.37(0.40)	1.31(0.32)	0.13(0.04)	...	9.18(2.23)	1.44(0.54)	...
G113.62+15.01a1	8.88	0.86	0.90	0.13	0.12	9.75(0.32)	10.92(0.58)	1.71(0.29)	0.26(0.06)	5.59(4.33)	11.84(2.03)	47.18(37.45)	...
G114.56+14.72a1	8.86	0.79	1.27	0.27	0.98	12.36(0.24)	34.85(1.01)	2.57(0.16)	0.57(0.19)	1.76(1.24)	4.77(3.31)	11.62(3.24)	3.21(11.06)
G114.67+14.47a1	8.85	0.77	2.10	0.27	0.98	12.36(0.24)	34.85(1.01)	3.08(0.50)	2.47(0.45)	0.88(3.19)	21.10(3.43)	11.72(2.86)	4.19(15.12)
G115.81-03.54a1	8.72	0.48	1.06	0.24	0.62	9.91(0.24)	8.22(0.34)	1.27(0.13)	1.33(0.28)	0.89(1.13)	8.46(0.86)	15.71(3.71)	10.47(13.41)
G115.92+09.46a1	8.98	1.00	0.99	0.17	10.75(0.18)	12.08(0.37)	0.61(0.29)	0.14(0.04)	...	4.30(2.05)	3.26(1.81)
G117.11+12.42a1	8.55	0.87	0.14	0.16	1.12	12.32(0.37)	14.38(0.80)	0.81(0.22)	0.36(0.08)	1.42(0.18)	5.16(1.43)	6.92(2.46)	27.46(35.71)
G120.16-03.09a1	9.26	1.36	0.90	0.18	...	15.79(0.19)	16.51(0.72)	5.47(0.29)	6.86(1.29)	4.77(3.31)	41.27(1.88)	11.55(8.05)	...
G120.67+02.66a1	9.56	1.82	0.62	0.11	...	16.90(0.26)	23.08(0.72)	2.00(0.31)	4.85(0.90)	1.32(0.88)	16.18(2.48)	29.98(7.22)	8.14(5.58)
G120.67+02.66a2	9.56	1.82	0.46	0.04	...	17.79(0.21)	21.36(0.47)	1.82(0.26)	6.50(1.20)	2.54(3.27)	14.75(2.08)	44.07(10.25)	17.19(22.33)
G120.98+02.66a1	8.98	0.87	0.78	0.14	2.48	15.10(0.30)	18.15(0.60)	2.32(0.27)	12.68(2.42)	1.71(0.34)	16.38(1.92)	77.40(17.35)	17.72(16.98)
G121.35+03.39a1	8.90	0.72	0.10	0.53	0.75	7.55(0.27)	7.51(0.42)	1.93(0.19)	1.47(1.46)	1.47(1.46)	13.40(0.32)	12.80(2.82)	11.00(10.97)
G122.01-07.48a2	5.39	0.74	0.11	0.09	12.17(0.24)	8.33(0.31)	0.74(0.14)	0.11(0.04)	...	10.22(1.88)	1.03(0.39)
G122.18-10.27a2	9.18	1.17	1.27	0.08	12.98(0.44)	8.03(0.44)	1.23(0.16)	0.16(0.05)	...	9.13(0.17)	1.80(0.63)
G125.66-00.55a1	8.80	0.55	0.17	0.63	12.58(0.14)	13.94(0.42)	2.24(0.23)	1.76(0.34)	1.57(1.39)	15.19(1.57)	11.60(2.51)	10.35(9.19)	...
G125.66-00.55a2	8.80	0.50	0.12	0.69	10.48(0.14)	15.52(0.47)	0.99(0.18)	1.83(0.36)	...	6.74(1.20)	27.14(7.24)
G125.66-00.55a2	8.80	0.50	0.48	...	0.42	10.48(0.14)	9.29(0.38)	0.74(0.17)	0.92(1.51)	7.55(0.31)	9.79(2.27)	12.18(19.99)	...
G125.66-00.55a1	8.80	0.50	0.37	...	0.25	11.34(0.15)	8.73(0.39)	0.62(0.16)	1.11(0.94)	7.10(0.31)	8.68(2.26)	15.64(13.20)	...
G126.27+05.11a1	9.31	1.27	0.91	0.21	...	10.48(0.54)	5.98(0.47)	0.76(0.14)	0.78(1.26)	5.83(0.07)	...	13.46(21.81)	...

Table 2 — Continued

Designation	R_{gal} (kpc)	Dist kpc	$\tau_{13\text{CO}}$	$\tau_{\text{C}^{18}\text{O}}$	τ_{HCO^+}	$T_{\text{ex}}^{\text{CO}}$ (K)	$N_{13\text{CO}}$ (10^{15}cm^{-2})	$N_{\text{C}^{18}\text{O}}$ (10^{15}cm^{-2})	N_{HCO^+} (10^{12}cm^{-2})	N_{HCN} (10^{12}cm^{-2})	N_{HCO^+} (10^{21}cm^{-2})	X_{HCN} (10^{-11})
G126.49-01.30a1	9.27	1.21	0.74	0.12	0.78	11.38(0.23)	14.73(0.54)	1.16(0.22)	2.34(0.46)	...	8.77(1.64)	26.67(7.23)
G126.49-01.30a2	9.27	1.21	0.63	0.32	11.22(0.32)	15.02(0.98)	2.09(0.46)	0.66(0.78)	13.40(0.88)	15.61(3.58)	4.94(5.84)	
G128.95-00.18a1	9.02	0.80	0.60	0.08	0.59	13.19(0.60)	9.44(0.66)	0.91(0.13)	1.77(0.44)	6.49(0.92)	6.49(0.91)	27.26(7.77)
G128.95-00.18a2	9.47	1.43	0.51	...	12.16(0.48)	7.52(0.52)	6.98(0.48)	...	8.63(10.45)	
G129.94+11.73a1	9.02	0.78	1.19	...	0.06	8.38(0.33)	7.38(0.78)	...	0.07(0.03)	...	6.26(0.66)	
G130.14+11.07a1	9.49	1.44	0.62	0.08	0.06	13.88(0.17)	15.51(0.40)	1.32(0.21)	0.10(0.03)	10.50(1.65)	1.18(0.53)	
G131.72+09.70a1	9.25	1.07	0.90	0.12	0.09	11.22(0.30)	11.83(0.52)	1.13(0.18)	0.14(0.05)	8.53(1.39)	0.99(0.37)	
G133.28+08.81a2	9.64	1.56	0.47	0.25	...	8.28(0.33)	5.11(0.53)	0.64(0.17)	...	5.25(0.36)	1.58(0.65)	
G133.28+08.81b1	9.64	1.56	0.24	...	14.41(0.90)	3.88(0.87)	0.28(0.29)	...	5.24(5.71)	
G133.28+08.81b2	9.30	1.11	0.92	0.12	0.43	11.80(0.38)	15.10(0.90)	1.17(0.23)	1.26(0.24)	3.72(0.83)	...	7.31(6.65)
G133.48+09.02a1	9.73	1.68	0.97	0.16	0.19	16.39(0.33)	47.36(1.46)	5.66(0.47)	1.33(0.26)	6.67(0.98)	47.66(3.94)	
G136.31-01.77a2	9.17	0.90	1.12	0.20	0.22	9.54(0.35)	9.50(0.54)	0.89(0.15)	3.75(0.75)	1.69(1.91)	5.7(1.09)	
G140.49-06.07a1	9.96	1.81	0.50	0.04	1.81	13.86(0.24)	13.95(0.43)	1.44(0.29)	6.33(0.75)	1.45(2.40)	12.77(2.59)	
G140.77+05.00a1	8.96	0.58	0.72	0.11	0.45	14.06(0.19)	13.46(0.32)	1.43(0.41)	1.12(0.32)	2.57(2.34)	10.06(2.86)	
G140.97+05.73a1	9.47	1.21	0.99	0.12	0.31	11.32(0.19)	13.14(0.38)	1.21(0.15)	0.97(0.25)	0.72(0.24)	9.57(1.16)	
G142.25+05.43a2	9.38	1.08	0.80	...	10.83(0.29)	6.14(0.32)	...	0.23(0.08)	...	5.60(0.29)	4.17(0.36)	
G142.29+07.65a1	9.67	1.43	0.57	...	0.68	11.56(0.45)	6.67(0.29)	0.57(0.14)	4.51(0.28)	12.68(3.25)	...	
G142.29+07.65a2	9.67	1.43	0.75	0.11	1.32	9.53(0.35)	4.14(0.24)	0.48(0.08)	2.64(0.51)	1.67(0.84)	3.97(0.70)	
G142.62+07.29a3	9.47	1.19	0.60	0.07	0.20	10.07(0.24)	4.80(0.24)	0.22(0.08)	0.52(0.16)	1.77(0.64)	29.50(13.83)	
G144.49+08.70a1	9.36	1.03	0.88	0.16	0.66	10.78(0.20)	8.69(0.27)	1.04(0.27)	1.12(0.29)	0.81(0.71)	8.01(2.11)	
G144.84+00.76a1	11.50	3.46	0.62	0.13	0.13	9.64(0.62)	11.37(1.51)	1.70(0.71)	2.29(0.29)	21.11(8.80)	1.36(0.68)	
G146.1+07.80a1	9.59	1.28	0.50	...	0.42	10.27(0.44)	5.21(0.41)	0.97(0.26)	4.95(0.39)	19.54(5.46)	...	
G146.1+07.80a2	9.59	1.28	1.01	0.19	0.38	9.54(0.20)	8.84(0.31)	0.89(0.11)	1.33(0.30)	0.89(3.28)	7.26(0.86)	
G146.1+07.80a3	9.59	1.28	0.99	0.15	1.24	9.39(0.29)	8.73(0.44)	0.69(0.13)	2.01(0.44)	1.25(1.00)	5.60(1.06)	
G146.18+08.80a2	9.46	1.13	1.04	0.45	0.45	8.86(0.25)	9.72(0.47)	1.09(0.18)	0.66(0.91)	8.39(0.45)	12.00(3.60)	
G146.71+02.05a3	0.42	...	0.18	0.50(0.13)	7.70(10.61)	
G146.7+02.05b1	1.25	...	0.39	0.88(0.19)	
G147.01+03.39a1	9.00	0.59	1.43	...	0.39	10.42(0.61)	6.79(0.59)	...	2.40(0.44)	2.16(0.69)	5.74(0.50)	
G147.76+09.17a1	9.75	1.44	0.86	0.16	0.77	11.43(0.50)	8.26(0.56)	0.96(0.16)	2.22(0.45)	8.12(1.37)	27.33(7.17)	
G148.00+00.09b1	12.42	4.36	0.81	0.21	0.19	6.93(0.50)	6.37(0.64)	0.50(0.12)	0.60(0.17)	0.41(0.21)	6.84(1.71)	
G148.00+00.09b1	9.15	0.76	0.50	0.12	...	14.11(0.64)	8.79(0.65)	0.54(0.13)	0.54(0.17)	0.54(0.97)	3.99(0.99)	
G148.00+00.09b2	12.41	4.36	0.72	0.07	0.18	10.47(0.68)	5.68(0.61)	0.28(0.12)	0.52(0.14)	0.88(0.71)	3.8(1.61)	
G148.00+00.09b2	9.15	0.76	0.60	0.05	0.17	12.77(0.55)	8.92(0.61)	0.35(0.14)	0.45(0.12)	2.58(1.03)	17.52(5.50)	
G148.00+00.09b3	9.16	0.77	0.65	0.09	0.50	10.43(0.64)	8.88(0.86)	0.95(0.20)	1.02(0.21)	1.71(1.77)	7.04(1.46)	
G148.00+00.09b3	9.16	0.77	0.41	0.18	0.18	12.93(0.51)	9.43(0.72)	...	0.27(0.09)	8.23(0.63)	3.25(1.14)	
G148.24+00.41a2	12.47	4.42	0.39	0.25	19.22(0.71)	18.51(1.14)	...	1.09(0.23)	0.89(1.47)	27.96(1.72)	3.88(0.87)	
G149.58+03.45a1	8.65	0.17	1.51	0.24	0.96	9.67(0.41)	13.85(0.88)	1.02(0.16)	1.20(0.27)	0.75(1.16)	6.67(1.72)	
G149.52-01.23a1	9.23	0.84	0.57	0.06	0.65	16.15(0.17)	22.03(0.42)	1.66(0.20)	3.28(0.64)	2.00(5.74)	12.45(1.53)	
G150.22+03.91a2	8.66	0.18	1.11	0.18	0.53	17.75(0.55)	9.18(0.71)	0.74(0.18)	0.79(0.19)	1.02(0.21)	7.04(1.46)	
G151.08+04.46a1	8.63	0.15	0.94	0.18	0.53	13.40(0.39)	11.44(0.54)	0.65(0.13)	0.76(0.15)	0.63(0.59)	4.24(0.84)	
G153.34-08.00a1	10.84	2.55	0.99	0.15	0.37	10.44(0.35)	9.23(0.52)	0.95(0.17)	1.08(0.26)	1.37(1.62)	10.20(1.81)	
G154.07+05.09a1	8.72	1.24	1.32	0.09	0.46	10.63(0.18)	18.31(0.50)	1.04(0.15)	1.02(0.24)	1.02(2.25)	6.95(0.98)	
G154.07+05.21a1	8.65	0.17	0.83	0.25	1.57	11.07(0.27)	11.31(0.44)	1.31(0.13)	2.79(0.56)	1.08(0.89)	8.61(0.87)	
G154.07+05.21a2	8.71	0.23	0.63	...	0.61	11.98(0.32)	9.13(0.49)	...	1.38(0.32)	1.56(1.51)	7.28(0.39)	
G154.90+04.61a1	8.74	0.26	0.93	0.06	4.05	13.33(0.23)	18.30(0.52)	0.94(0.19)	7.22(1.40)	3.22(2.37)	6.31(1.24)	
G155.67+05.11b2	8.79	0.32	1.10	0.13	0.39	11.14(0.25)	13.50(0.56)	0.76(0.17)	0.85(0.26)	1.02(1.64)	5.7(0.74)	
G156.04+06.03a2	8.92	0.46	1.20	0.26	0.72	10.33(0.56)	8.95(0.73)	0.69(0.14)	1.61(0.32)	1.25(0.28)	5.8(0.61)	
G156.04+06.03a3	8.92	0.46	0.89	...	0.72	10.33(0.69)	6.97(0.74)	...	1.25(0.28)	...	5.8(0.61)	
G156.20+05.26b1	8.90	0.43	1.06	0.06	1.24	10.37(0.29)	7.25(0.39)	...	2.28(0.49)	...	6.00(0.33)	
G156.20+05.26b2	8.90	0.43	1.72	0.17	...	10.53(0.38)	9.89(0.53)	0.80(0.11)	3.2(0.60)	2.10(2.18)	5.55(0.77)	
G157.12-11.56a1	8.63	0.14	0.85	0.14	0.58	12.17(0.28)	10.42(0.37)	1.19(0.12)	1.74(0.40)	...	5.12(1.12)	
G157.12-11.56a2	8.63	0.14	0.75	0.11	0.41	12.23(0.24)	9.46(0.30)	1.05(0.12)	1.21(0.31)	...	16.58(6.21)	
G157.60-12.17a1	8.63	0.14	0.46	0.10	1.50	16.26(0.29)	10.96(0.55)	1.76(0.17)	2.36(0.49)	2.09(0.77)	11.47(0.69)	
G157.60-12.17b2	8.94	0.47	0.22	...	16.64(0.38)	7.52(0.51)	...	1.11(0.31)	6.28(0.42)	6.28(0.42)	17.60(48.00)	
G158.22-20.14a2	9.30	0.86	0.82	0.14	1.12	16.00(0.29)	16.55(0.50)	1.66(0.20)	2.08(0.38)	1.26(0.35)	16.41(3.64)	9.93(3.01)

Table 2 — *Continued*

Table 2 — Continued

Designation	R_{gal} (kpc)	Dist kpc	$\tau_{13\text{CO}}$	$\tau_{\text{C}^{18}\text{O}}$	τ_{HCO^+}	$T_{\text{ex}}^{\text{CO}}$ (K)	$N_{13\text{CO}}$ (10^{15}cm^{-2})	$N_{\text{C}^{18}\text{O}}$ (10^{15}cm^{-2})	N_{HCO^+} (10^{12}cm^{-2})	N_{HCN} (10^{12}cm^{-2})	N_{HCO^+} (10^{11}cm^{-2})	X_{HCN} (10^{-11})
G173.12-13.32a1	9.96	1.47	1.15	...	10.91(0.63)	11.45(1.19)	...	0.38(0.08)	0.28(1.11)	11.71(1.22)	...	2.39(9.46)
G173.36-16.27a1	10.31	1.82	1.09	0.64	0.37	14.82(1.22)	25.14(4.80)	7.40(1.65)	0.38(0.08)	70.90(15.78)	0.53(0.17)	...
G173.60-17.89a1	9.71	1.22	0.75	0.11	0.23	10.16(0.24)	7.40(0.33)	0.38(0.10)	0.79(0.23)	3.18(0.88)	24.74(9.84)	...
G173.89-17.64a2	8.73	0.23	0.98	...	0.24	11.58(1.34)	12.10(2.49)	...	0.21(0.17)	9.69(2.00)	2.17(1.77)	...
G173.95-13.74a1	8.73	0.23	1.17	0.38	1.29	14.44(0.62)	27.62(1.83)	6.37(0.64)	1.66(0.31)	0.57(0.18)	42.48(4.26)	3.92(0.84)
G174.06-15.81a1	10.46	1.97	1.08	0.20	...	14.21(0.33)	21.61(0.83)	2.08(0.25)	1.29(0.50)	1.29(0.50)	20.60(2.52)	11.64(2.54)
G174.44-15.75a1	8.73	0.23	0.99	0.20	3.24	14.17(0.60)	18.21(1.28)	2.39(0.42)	4.54(0.83)	0.90(0.79)	15.97(2.78)	28.45(7.20)
G174.70-15.48a1	8.73	0.23	1.42	0.40	...	12.98(0.23)	18.00(0.52)	2.56(0.15)	4.02(0.73)	1.86(1.39)	17.07(0.98)	23.54(4.48)
G175.16-16.74a2	10.69	2.20	2.18	0.17	0.09	8.69(0.40)	14.84(0.99)	0.57(0.13)	0.14(0.05)	...	5.90(1.35)	2.29(1.01)
G175.49-16.80a2	8.73	0.23	1.10	...	0.08	10.34(0.47)	13.82(0.98)	...	0.39(0.11)	...	11.07(0.78)	3.50(1.05)
G175.97-20.38a1	11.58	3.09	0.95	...	0.36	9.29(0.35)	6.40(0.41)	...	0.31(0.10)	...	8.94(0.57)	3.44(1.16)
G176.94+04.63a1	1.76	...	0.10	0.20(0.08)
G177.14-01.21a1	8.67	0.17	1.02	0.14	...	12.15(0.21)	23.65(0.69)	3.19(0.33)	0.27(0.65)	21.00(2.20)	...	1.26(3.08)
G177.62-20.36a1	8.73	0.23	0.88	...	0.47	11.03(0.54)	16.10(1.23)	...	0.40(0.09)	...	12.89(0.98)	3.07(0.73)
G178.28-00.61a2	10.02	1.52	0.78	0.11	0.12	12.67(0.17)	16.41(0.41)	1.60(0.18)	0.38(0.11)	...	14.35(1.62)	2.66(0.85)
G180.92+04.53a1	12.12	3.62	0.81	0.16	0.53	9.68(0.24)	9.85(0.47)	0.84(0.18)	1.66(0.42)	6.46(14.96)	11.58(2.43)	14.36(4.71)
G181.16-04.33a1	14.86	0.78	0.22	0.88	10.73(0.20)	9.01(0.48)	0.61(0.36)	1.66(0.36)	0.84(0.12)	19.96(6.44)	10.11(25.56)	
G181.16+04.33a2	14.86	0.68	0.15	0.40	10.58(0.18)	13.59(0.49)	0.94(0.16)	1.43(0.31)	2.29(1.01)	12.95(2.22)	11.03(3.04)	
G181.42-03.73a1	12.48	3.98	0.85	0.07	1.35	13.26(0.39)	11.97(0.63)	1.90(0.43)	3.29(0.63)	1.06(1.98)	26.22(5.88)	12.57(3.71)
G181.7+04.16a1	17.67	9.83	0.11	0.80	9.24(0.25)	8.57(0.42)	0.71(0.17)	1.15(0.29)	...	9.83(2.35)	11.65(4.07)	...
G181.84+00.31a1	17.49	8.99	0.66	...	9.16(0.61)	4.91(0.56)	...	0.51(3.90)	...	7.42(0.84)	...	6.92(52.60)
G181.84+00.31a2	17.49	8.99	0.64	...	10.54(0.48)	6.60(0.50)	...	2.58(0.48)	2.64(1.68)	9.97(1.73)	25.90(5.23)	
G181.84+00.31b1	17.49	8.99	0.58	...	0.90	9.70(0.40)	5.77(0.41)	...	1.50(0.32)	1.03(1.69)	8.71(0.61)	17.26(3.87)
G181.84+00.31b2	17.49	8.99	0.70	...	11.04(0.40)	11.10(0.67)	...	1.15(0.30)	3.16(0.66)	16.76(1.01)	20.98(4.13)	
G182.04+00.41b1	14.01	5.51	0.83	...	0.65	10.78(0.45)	11.73(1.01)	...	1.43(0.79)	17.72(1.52)	11.11(2.51)	8.09(4.50)
G185.29-02.27a1	8.74	0.24	0.61	0.46	0.46	8.19(0.35)	8.77(0.75)	...	1.05(0.25)	7.04(0.61)	14.99(3.75)	...
G185.80-09.12a1	9.38	0.88	0.92	0.14	...	13.30(0.21)	12.06(0.33)	0.99(0.12)	2.63(0.49)	1.21(1.56)	7.68(0.93)	34.20(7.61)
G185.80-09.12a2	9.38	0.88	1.02	0.08	0.43	12.67(0.31)	9.65(0.40)	1.53(0.25)	1.15(0.30)	...	11.88(1.94)	9.68(2.95)
G190.08-13.51a2	8.96	0.47	0.72	0.13	0.38	12.45(0.23)	11.94(0.45)	1.25(0.19)	1.03(0.28)	0.59(0.17)	8.78(1.34)	11.78(3.64)
G190.08-13.51a4	8.96	0.51	0.83	...	0.65	10.78(0.45)	11.73(1.01)	...	0.28(0.08)	1.27(4.39)	8.58(0.32)	3.24(0.85)
G190.17-13.78a1	8.92	0.43	0.78	0.08	0.08	14.60(0.98)	16.31(1.64)	...	0.36(0.11)	0.44(0.63)	13.58(1.37)	2.63(0.85)
G190.15-14.34a1	8.72	0.22	0.60	...	0.28	15.52(0.20)	11.70(0.31)	...	0.94(0.21)	1.03(0.71)	9.35(0.25)	10.02(2.29)
G190.15-14.34a2	8.72	0.22	0.73	0.06	0.39	15.75(0.19)	14.41(0.33)	1.01(0.15)	1.18(0.28)	1.40(1.44)	6.73(0.99)	17.51(4.95)
G190.15-14.34a3	8.97	0.46	0.66	...	0.28	12.45(0.23)	13.39(0.49)	...	0.51(0.19)	2.38(2.37)	11.26(0.41)	14.62(3.21)
G191.03-16.74a1	9.06	0.57	0.71	0.16	0.17	14.79(0.30)	9.84(0.34)	1.12(0.16)	0.61(0.17)	1.25(1.12)	8.06(1.15)	7.58(1.51)
G191.5-10.76a2	8.68	0.18	0.99	0.07	14.11(0.66)	16.58(1.20)	2.12(0.35)	0.21(0.08)	0.36(0.11)	13.58(1.37)	3.28(4.62)	
G192.12-10.96a1	8.89	0.40	0.81	0.15	0.61	18.67(0.32)	16.43(0.47)	1.97(0.17)	1.32(0.29)	1.11(1.53)	13.65(1.19)	11.06(7.58)
G192.12-10.96a2	11.23	2.78	0.70	0.06	0.75	19.10(0.36)	18.38(0.62)	1.25(0.27)	2.45(0.49)	1.57(1.61)	14.62(3.21)	20.87(21.61)
G192.12-10.96a3	11.23	2.78	0.65	...	0.34	22.15(0.58)	21.76(1.13)	...	1.94(0.42)	2.38(3.48)	11.26(0.41)	16.75(4.98)
G192.28-11.33a1	11.24	2.79	0.94	0.13	0.22	18.34(0.43)	18.13(0.78)	2.64(0.49)	0.26(0.04)	1.25(1.12)	8.06(1.53)	15.52(14.03)
G192.28-11.33a2	11.24	0.77	0.13	0.59	20.82(0.37)	18.67(0.63)	1.62(0.28)	2.38(0.48)	1.42(1.50)	13.95(2.28)	1.49(0.64)	
G192.28-11.33a3	11.24	0.96	0.10	1.27	21.47(0.21)	28.16(0.47)	2.39(0.22)	3.87(0.74)	1.42(1.50)	27.99(2.56)	13.84(2.92)	
G192.32-11.87a1	11.87	3.43	0.53	...	0.19	17.91(0.29)	16.56(0.48)	...	0.51(0.11)	0.60(0.25)	24.43(0.71)	20.76(11.26)
G192.54-11.56a1	11.20	2.75	0.51	0.06	0.88	34.43(0.37)	26.62(0.56)	2.68(0.39)	1.53(0.35)	1.02(1.77)	31.21(4.58)	3.25(5.69)
G194.80-03.41a1	11.32	2.89	1.59	0.00	1.00	10.59(0.37)	26.29(1.49)	2.29(0.64)	1.01(0.23)	3.17(1.30)	27.30(7.68)	38.85(13.22)
G195.09-16.41a1	8.89	0.40	0.64	0.17	0.41	14.80(0.22)	16.01(0.31)	1.27(0.11)	0.98(0.25)	0.51(0.54)	11.15(2.99)	...
G195.09-16.95a1	8.89	0.40	0.86	0.14	0.83	16.49(0.23)	25.24(0.63)	3.08(0.26)	1.80(0.38)	1.38(1.89)	21.31(1.81)	8.43(1.94)
G195.09-16.95a2	8.89	0.40	0.73	0.12	0.48	16.53(0.24)	18.33(0.55)	1.85(0.25)	0.85(0.25)	0.59(0.18)	12.82(1.72)	6.62(2.14)
G196.21-15.56a1	8.88	0.40	0.35	...	0.22	15.92(0.23)	10.83(0.33)	...	0.59(0.18)	1.16(1.75)	8.95(0.28)	6.61(2.01)
G198.03-15.24a1	8.63	0.14	1.00	...	0.22	15.19(0.47)	12.90(0.61)	...	0.58(0.16)	3.02(2.70)	10.14(0.48)	5.68(1.64)
G198.03-15.24a2	8.63	0.14	0.73	0.09	0.31	14.14(0.27)	8.78(0.35)	0.72(0.15)	0.40(0.11)	0.51(0.54)	8.79(0.79)	11.15(2.99)
G198.56-09.10a1	8.93	0.45	0.77	0.12	1.95	16.23(0.34)	16.01(0.60)	1.87(0.27)	6.04(1.15)	1.63(1.17)	13.07(1.87)	46.22(10.99)
G199.88-00.93a1	9.42	0.97	1.35	0.39	0.66	9.33(0.15)	19.54(0.59)	2.07(0.19)	1.26(0.29)	1.47(1.11)	16.71(1.46)	7.76(1.90)
G200.34-10.97a1	10.66	2.27	1.01	0.13	0.27	12.61(0.33)	9.87(0.42)	0.53(0.12)	0.82(0.21)	0.55(0.24)	14.79(5.01)	9.06(6.94)
G200.34-10.97a2	10.66	2.27	0.88	0.14	0.87	13.82(0.40)	9.20(0.45)	0.62(0.13)	0.74(1.40)	6.38(1.33)	32.29(3.37)	11.59(22.04)
G200.34-10.97a3	10.66	2.27	1.05	0.15	0.80	13.27(0.37)	14.11(0.64)	1.19(0.19)	1.04(2.38)	1.65(0.37)	12.35(0.93)	8.47(19.33)

Table 2 — *Continued*

Designation	R_{gal} (kpc)	Dist kpc	$\tau_{13\text{CO}}$	$\tau_{\text{C}^{18}\text{O}}$	τ_{HCO^+}	$T_{\text{ex}}^{\text{CO}}$ (K)	$N_{13\text{CO}}$ (10^{15} cm^{-2})	$N_{\text{C}^{18}\text{O}}$ (10^{15} cm^{-2})	N_{HCO^+} (10^{12} cm^{-2})	N_{HCN} (10^{12} cm^{-2})	N_{H_2} (10^{21} cm^{-2})	X_{HCN} (10^{-11})	
G201.13+00.31b1	9.24	0.79	1.47	0.15	...	11.34(0.46)	16.38(1.02)	1.14(0.27)	3.03(0.56)	2.09(5.04)	8.55(2.04)	35.41(1.72)	
G201.26+00.46b2	9.35	0.91	0.72	0.09	...	11.20(0.21)	11.11(0.43)	0.76(0.17)	0.53(2.18)	5.88(1.32)	28.39(1.30)	7.63(1.60)	
G201.44+00.65a2	9.00	0.53	0.92	0.31	12.48(0.32)	33.61(1.54)	...	2.17(0.44)	...	10.48(2.62)	22.09(7.52)	...	
G201.59+00.55a1	9.14	0.68	0.82	0.11	0.34	12.39(0.28)	29.49(1.11)	1.43(0.36)	2.32(0.53)	
G202.21-09.17a2	8.89	0.41	0.91	0.05	...	12.01(0.28)	12.03(0.47)	0.54(0.18)	1.07(7.20)	3.72(1.21)	11.61(3.20)	28.79(193.94)	
G202.30-08.91a1	8.89	0.41	1.15	0.25	0.31	12.12(0.26)	17.77(0.75)	1.99(0.19)	1.60(0.41)	...	13.78(1.30)	...	
G202.30-08.91b2	8.89	0.41	1.31	0.24	0.42	10.87(0.31)	18.21(0.95)	2.25(0.22)	0.70(0.19)	...	15.60(1.51)	4.51(1.29)	
G202.30-08.91b3	8.89	0.41	1.16	0.35	0.66	11.52(0.26)	17.14(0.78)	2.46(0.20)	1.45(0.31)	3.47(2.94)	17.05(0.40)	8.52(1.97)	
G203.20-11.20a1	8.88	0.41	1.26	0.28	0.80	12.93(0.33)	22.08(0.87)	3.88(0.29)	0.81(0.22)	1.90(5.38)	26.83(1.99)	3.03(0.85)	
G203.75-08.49a1	8.86	0.39	1.02	0.14	0.31	10.35(0.27)	10.46(0.48)	0.43(0.12)	1.10(0.28)	...	2.95(0.86)	37.26(14.38)	
G204.49-11.33a1	8.80	0.33	1.34	0.08	13.67(0.95)	17.49(2.11)	...	0.24(0.09)	0.32(1.20)	14.21(1.72)	1.68(0.64)	2.28(8.45)	
G204.49-11.33a2	8.88	0.41	0.94	0.16	0.08	16.03(0.97)	16.93(1.56)	2.10(0.54)	0.28(0.09)	...	14.48(3.71)	1.96(0.80)	...
G204.82-13.88a1	8.88	0.41	0.72	0.10	0.43	18.68(0.21)	34.26(0.72)	2.10(0.24)	2.79(0.57)	1.80(3.25)	14.53(0.67)	19.24(4.53)	12.39(22.42)
G206.87-04.36a1	8.87	0.41	0.73	...	13.36(0.39)	15.34(0.89)	2.27(2.07)	12.64(0.74)	...	17.99(16.39)	
G207.35-19.82a1	8.87	0.41	0.81	0.15	0.15	20.84(0.17)	34.63(0.53)	4.24(0.23)	4.76(0.88)	3.13(1.58)	29.28(1.60)	16.27(3.13)	
G207.35-19.82a2	9.93	1.58	0.98	0.13	...	19.83(0.20)	40.80(0.75)	4.45(0.37)	9.92(1.78)	16.15(2.62)	39.15(3.27)	25.33(5.02)	
G215.4-16.39a1	8.84	0.41	0.88	0.14	0.72	11.17(0.30)	8.45(0.44)	0.64(0.15)	1.27(0.27)	0.75(0.88)	4.37(1.04)	29.01(9.24)	
G215.70-15.05a1	9.71	1.44	0.58	...	10.55(0.35)	7.66(0.48)	...	3.56(2.80)	1.34(2.21)	7.45(0.47)	47.74(37.68)	18.01(29.67)	
G215.88-17.58a1	9.46	1.15	1.19	0.22	0.55	14.26(0.34)	19.18(0.85)	2.58(0.35)	1.42(0.32)	...	20.39(2.79)	6.97(1.82)	...
G217.13-12.55a1	8.83	0.41	0.79	0.16	...	10.38(0.27)	12.63(0.59)	1.14(0.20)	1.8(0.37)	1.60(1.69)	7.78(1.40)	23.24(6.36)	
G217.46-13.78a1	8.83	0.41	0.91	0.16	0.68	11.71(0.28)	8.73(0.39)	0.92(0.15)	2.19(0.54)	1.64(2.67)	6.26(1.02)	34.98(10.37)	
G217.70-16.12a1	9.00	0.62	1.41	7.69(0.31)	7.07(0.50)	1.17(3.04)	5.97(0.42)	...	
G224.47-00.65a1	9.65	1.52	0.44	...	0.50	13.74(1.07)	14.00(2.37)	...	1.32(0.39)	0.67(1.17)	13.46(2.28)	9.78(3.33)	
G226.29-00.63a1	9.76	1.71	1.81	11.92(0.57)	37.24(4.60)	...	7.38(1.36)	13.85(2.53)	36.58(4.52)	20.16(4.48)	
G226.36-00.50a1	9.54	1.43	1.01	0.23	4.05	13.20(0.38)	21.81(1.29)	1.97(0.51)	24.16(4.56)	...	15.88(4.10)	152.15(48.64)	

Table 3
Statistics of Derived Parameters

	$N_{^{13}\text{CO}}$ (10^{15} cm^{-2})	$N_{\text{C}^{18}\text{O}}$ (10^{15} cm^{-2})	N_{HCO^+} (10^{12} cm^{-2})	N_{HCN} (10^{12} cm^{-2})	N_{H_2} (10^{21} cm^{-2})	$X_{^{13}\text{CO}}/X_{\text{C}^{18}\text{O}}$	X_{HCO^+} (10^{-11})	X_{HCN} (10^{-11})	$X_{\text{HCO}^+}/X_{\text{HCN}}$
Min.	3.77	0.22	0.07	0.24	1.45	3.40	0.30	1.26	0.05
Max.	56.63	8.68	24.16	16.15	70.90	36.56	152.15	55.81	5.07
Median	11.95	0.94	0.76	0.62	8.93	12.49	8.51	20.55	1.84
Mean	15.27	1.79	1.69	1.57	12.76	11.45	14.86	13.56	1.40
STD	9.41	1.42	2.73	1.91	9.82	5.33	18.79	10.90	0.99

Table 4
Statistics of Some Parameters of PGCCs

	N_{H_2} (10^{20} cm^{-2})	T_{dust} (K)	M_{clump} (M_\odot)	L_{clump} (L_\odot)
All PGCCs				
Min.	0.07	8.55	0.05	0.01
Max.	1189.23	30.00	1.26×10^5	2.92×10^6
Median	4.12	14.53	4.55	2.56
Mean	10.72	14.60	797.29	2299.61
STD	25.58	1.98	4771.02	52018.39
PGCCs detected in dense gas tracers				
Min.	2.52	9.20	0.80	0.37
Max.	136.95	14.52	4428.39	1567.50
Median	24.53	12.35	14.31	4.33
Mean	32.28	12.22	121.76	42.65
STD	25.21	1.13	532.11	188.13
PGCCs not detected in dense gas tracers				
Min.	2.65	9.20	0.54	0.30
Max.	156.91	17.31	3650.42	756.06
Median	15.30	12.29	8.04	3.03
Mean	20.72	12.32	176.56	38.31
STD	21.13	1.27	713.28	147.51

Note. — All the parameters are from the PGCC catalog ([Planck Collaboration et al. 2015](#)).